Journal of Structural Geology 37 (2012) 181–199

Contents lists available at SciVerse ScienceDirect

Journal of Structural Geology

journal homepage: www.elsevier.com/locate/jsg

Development and distribution of bed-parallel compaction bands and pressure solution seams in carbonates (Bolognano Formation, Majella Mountain, Italy)

Andrea Rustichelli [a,*], Emanuele Tondi [a], Fabrizio Agosta [b], Antonino Cilona [a], Maurizio Giorgioni [c]

[a] Geology Division, School of Science and Technology, University of Camerino, Via Gentile III da Varano, 62032 Camerino, Macerata, Italy
[b] Department of Geological Sciences, University of Basilicata, Potenza, Italy
[c] Shell Italia E&P, Rome, Italy

ARTICLE INFO

Article history:
Received 7 July 2011
Received in revised form
29 December 2011
Accepted 20 January 2012
Available online 31 January 2012

Keywords:
Carbonate reservoir
Apulian platform
Burial-related structures
Mechanical Layering
Fractures distribution

ABSTRACT

The Oligo-Miocene carbonates pertaining to the Bolognano Formation, cropping out at the Majella Mountain, Italy, are diffusely crosscut by bed-parallel structural elements such as compaction bands and pressure solution seams. These bed-parallel structural elements formed under a vertical loading, during the progressive burial of the carbonates. The present work focuses on the control exerted on their development and distribution by compositional, sedimentological and pore network characteristics of the studied carbonates. The main results are consistent with the following statements: (i) bed-parallel compaction bands developed only within the poorly cemented, porous grainstones (2D porosity > 10%; 3D porosity > 15%); (ii) distribution of these bands was strongly controlled by both sorting and sphericity of the carbonate grains, as well as by the amount of intergranular macroporosity; (iii) bed-parallel pressure solution seams formed, mainly, within the fine-grained packstones, which are characterized by small amounts of clayish matrix (2–4% of total rock volume), and well-sorted, spherical carbonate grains.

Considering the impact that burial-related, bed-parallel structures may have on fluid flow, the results provided in this contribution can help the management of subsurface geofluids, and overall prediction of carbonate reservoir quality, by mapping/simulating/assessing carbonate facies.

1. Introduction

Carbonate rocks are subject, during their burial history, to complex interactions between overburden-related conditions (i.e., stress field, pressure and temperature, fluid composition) and rock rheology (e.g. Bathurst, 1995; Bjørlykke and Høeg, 1997; Brown, 1997). These interactions can be responsible for the development of bed-parallel structural elements, such as compaction bands and pressure solution seams, which usually nucleate and grow during diagenesis within sub-horizontal sedimentary beds (Fig. 1; Zhang and Spiers, 2005; Aydin et al., 2006; Aydin and Ahmadov, 2009). The aforementioned bed-parallel structures commonly represent the oldest structural elements in carbonates. Although bed-parallel compaction bands and pressure solution seams form thanks to dissimilar deformation mechanisms, and develop in rocks characterized by different petrophysical properties (Aydin et al., 2006; and references therein), from a mechanical point of view they can both be treated as contractional structures (anti-mode I) that develop perpendicular to the maximum principal stress axis (Fletcher and Pollard, 1981).

Compaction bands are documented both in sandstones (Mollema and Antonellini, 1996; Aydin et al., 2006; Aydin and Ahmadov, 2009; Eichhubl et al., 2010) and carbonates (Tondi et al., 2006, in press; Antonellini et al., 2008; Agosta et al., 2009; Cilona et al., submitted for publication). In both cases, the localized strain that accumulates within narrow, elongated and sharp bands is the results of a slow ductile/brittle process (compaction banding) operating in the upper crust within unconsolidated, or slight consolidated, granular materials (Aydin, 1978; Antonellini and Aydin, 1994; Baud et al., 2004, 2009; Tondi et al., 2006; Fossen et al., 2007; Tondi, 2007; Aydin and Ahmadov, 2009; Vajdova et al., 2010; Cilona et al., submitted for publication; Vajdova et al., in press). In sandstones, compaction bands may have different orientations with respect to bedding (Eichhubl et al., 2010; and references therein); their documented micromechanisms include grain translation, rotation, pore collapse and grain crushing (Fig. 1a) due to Hertzian forces localized at a grain-to-grain scale (Gallagher, 1987; Zhang et al., 1990; Baud et al., 2000; Vajdova et al., 2004; Zhu et al., 2010; Brzesowsky et al.,

* Corresponding author.
E-mail address: andrea.rustichelli@unicam.it (A. Rustichelli).

0191-8141/$ – see front matter © 2012 Elsevier Ltd. All rights reserved.
doi:10.1016/j.jsg.2012.01.007

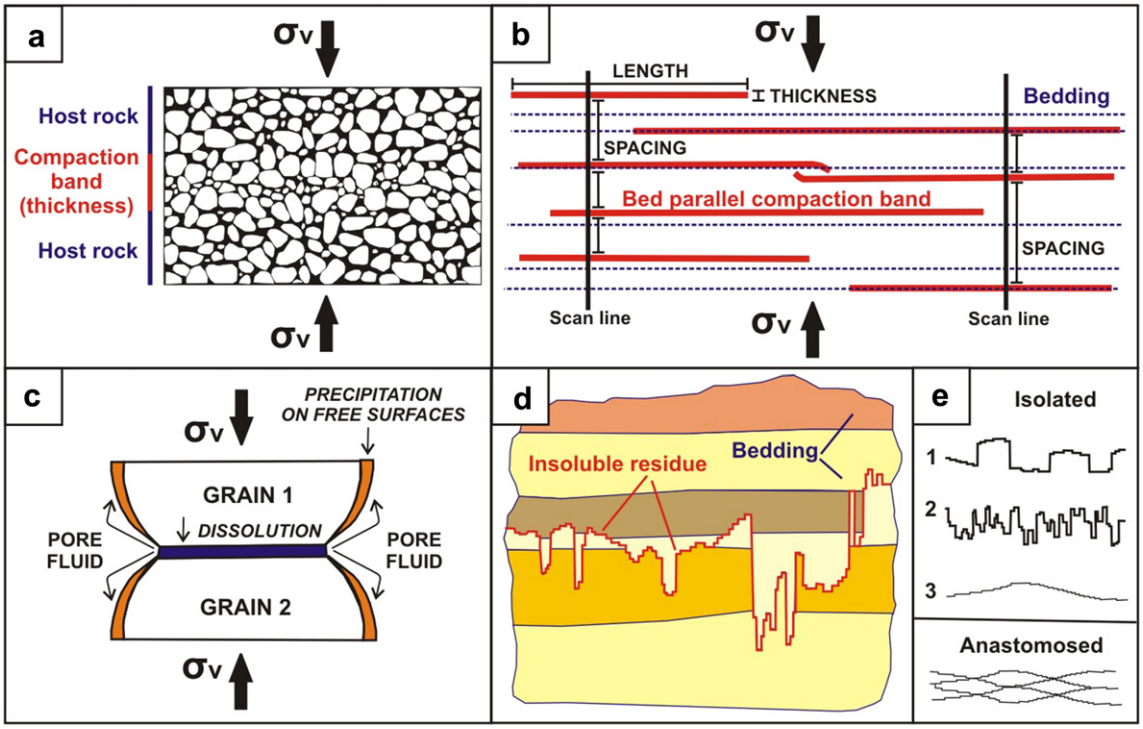

Fig. 1. Microscale processes responsible for development of either bed-parallel pressure solution seams or compaction bands, and their features at the macroscale. a) Compaction banding mechanism occurring in porous granular media (modified after Aydin et al., 2006). b) Two-dimensional cross-sectional views of bed-parallel compaction bands at outcrop scale (modified after Aydin and Ahmadov, 2009). c) Intergranular pressure solution mechanisms (modified after Zhang and Spiers, 2005). d) Two-dimensional cross-sectional views of bed-parallel pressure solution seams at outcrop scale. e) Different types (1, 2 and 3) and patterns (isolated versus anastomosed structures) of pressure solution seams. The method used to measure spacing (valid for both bed-parallel structures) is shown in b.

2011). In carbonates, compaction bands have been previously documented in the field oriented exclusively parallel to bedding, either within individual beds or adjacent to bedding interfaces (Tondi et al., 2006). Recently, discrete compaction bands were formed artificially in laboratory experiments, accompanied by randomly oriented tiny cracks nucleating at the grain contacts (Cilona et al., submitted for publication).

Pressure solution is a slow, ductile process operating in the upper and middle crust (diagenetic and low grade metamorphic conditions, Rutter, 1976; Paterson, 1995). This process is evident in sedimentary rocks, especially carbonates, at scales ranging from μm-to-cm (intergranular dissolution) to 10's μm-to-m (pressure solution seams; Bathurst, 1958). Often, this process is associated with mineral precipitation within nearby pores and/or fractures. The material removed is transported in solution by the dissolving fluids and, eventually, precipitates as cement either close to the dissolution sites (Fig. 1c) or at distances up to several Km's (Park and Schot, 1968; Agosta and Kirschner, 2003; Agosta et al., 2008). The resulting pressure solution seams commonly consist of serrated, interlocked, tooth-like surfaces made up of several columns and troughs, which can be either isolated or anastomosed (Fig. 1d and e). The columns and troughs are characterized in cross section by a typical zig-zag morphology; the former ones represent the zones of localized dissolution whereas the latter ones represent the undissolved portions of the rock consisting of clayish insoluble residues, organic matter and/or pods of undissolved grains (Bathurst, 1993). Outcrop observations, as well as theoretical and experimental studies, show that the main controls on pressure solution are the amount of stress, temperature, pore fluid chemistry and pressure, grain mineralogy, size, sorting and shape (Schmoker and Halley, 1982; Halley and Schmoker, 1983; Passchier and Trouw, 1996; Ehrenberg and Nadeau, 2005; Ehrenberg, 2006; Ehrenberg et al., 2009).

In this work, it is investigated the role exerted by compositional, sedimentological and pore network characteristics of carbonates on the development and distribution of both bed-parallel compaction bands and pressure solution seams. The present field and laboratory study is, therefore, aimed at the assessment of the relationships among the intrinsic characteristics of a variety of carbonate lithofacies (i.e., skeletal grainstones to packstones, marly wackestones to mudstones) and both presence and distribution of the bed-parallel structures in the Oligo-Miocene Bolognano Formation (Majella Mountain, Italy).

The results may have important applications in the management of subsurface geofluids. It is well-known, in fact, that bed-parallel compaction bands and pressure solution seams form permeability barriers to fluid flow (Aydin, 2000; Davison et al., 2000; Tondi, 2007; Agosta et al., 2010), and may act as mechanical interfaces in layered media (Huang and Angelier, 1989; Gross et al., 1995; Agosta et al., 2009).

2. Geological setting

The study area is located along the northern flank of the Majella Mountain, Italy. This mountain consists of an east-verging, box-shaped anticline comprised of Meso-Cenozoic carbonates of the paleo Apulian Platform (Fig. 2). This anticline fold formed, during the Middle-Upper Pliocene, at the hanging wall of a west-dipping thrust (Ghisetti and Vezzani, 2002). The western portion of the Majella Mountain, which corresponds to the anticline's backlimb, is crosscut by a major normal fault named Caramanico Fault (Vezzani and Ghisetti, 1998). In addition to this fault, the Majella Mountain is crosscut by several sets of normal, reverse and strike-slip faults, some which are characterized by oblique-slip components (Graham et al., 2003; Marchegiani et al., 2006;

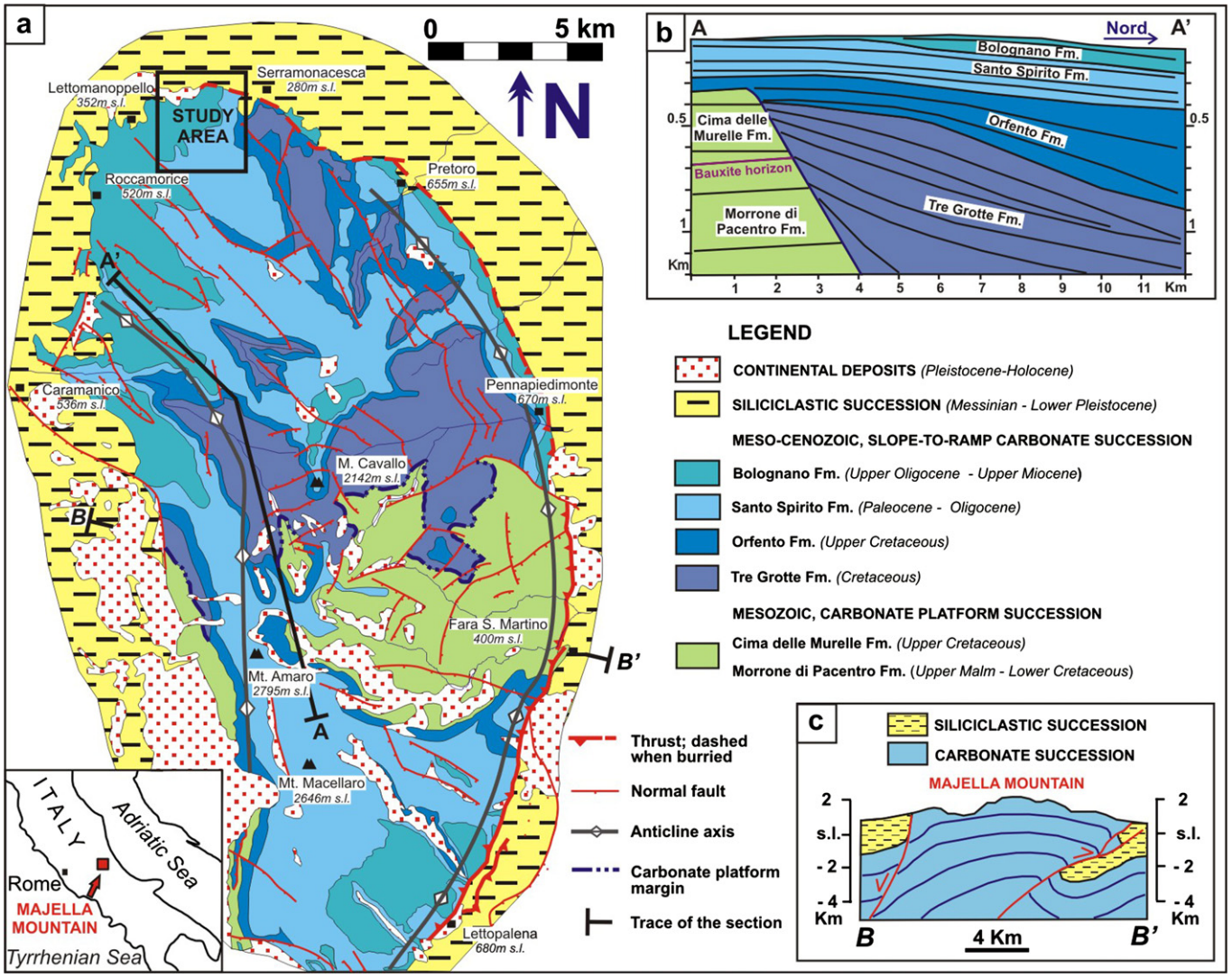

Fig. 2. Geological setting of Majella mountain. a) Schematic geological map (modified after Ghisetti and Vezzani, 1997). b) Stratigraphic scheme of the carbonate succession (modified after Vecsei, 1991). c) Schematic geological section (modified after Scisciani et al., 2002).

Tondi et al., 2006; Antonellini et al., 2008; Agosta et al., 2009; Aydin et al., 2010). Based upon crosscutting relationships with Messinian-to-Pleistocene sediments topping the carbonates, most of the faulting activity in the Majella Mountain is interpreted to have occurred during the Middle-Upper Pliocene (Ghisetti and Vezzani, 2002) or, alternatively, the Messinian (Scisciani et al., 2002). Detailed analysis of the deformation mechanisms associated with folding and faulting are consistent, for the northernmost portion of the Majella, with a Middle Pliocene age of faulting (Agosta et al., 2009).

The study was carried out along the vertical walls of the Roman Valley Quarry, and vertical outcrops in areas nearby, which are located in the northern slopes of the Majella Mountain near the town of Lettomanoppello (Figs. 2 and 3). There, the Oligo-Miocene ramp carbonate deposits of the Bolognano Formation, which represents the most recent stratigraphic unit of the Majella carbonate succession (Vecsei and Sanders, 1999) and references therein, crops out extensively. These carbonate rocks include skeletal grainstones, packstones, marly wackestones and mudstones. At the Roman Valley Quarry, the Bolognano Fm. is crosscut by two NW-SE-trending oblique-slip normal faults characterized by minor left-lateral components of slip; the oil show located in the quarry suggests the occurrence of hydrocarbon migration through the fault damage zones (Agosta et al., 2009, 2010).

3. Methodology

The results presented in this work required an integrated field and laboratory investigation to obtain, both qualitatively and quantitatively, an exhaustive characterization of the outcropping bed-parallel structural elements and the carbonate rocks in which these elements developed. This research takes advantage of the results of a recent project focused on the roles played by sedimentological and diagenetic factors on preservation and modification of pore network characteristics (i.e. porosity type, estimates and distribution) in the carbonates of the Bolognano Formation (Rustichelli, 2010).

The field work component of the current research included three main phases: (i) qualitative macroscopic analysis of the bed-parallel structural elements by detailed outcrop analysis accomplished by taping acetated to the studied walls; (ii) measurement of the different dimensional parameters (e.g., spacing, length, thickness) of the bed-parallel structures by performing 1D scan lines oriented perpendicular to bedding (Fig. 1B; Ortega et al., 2006), was

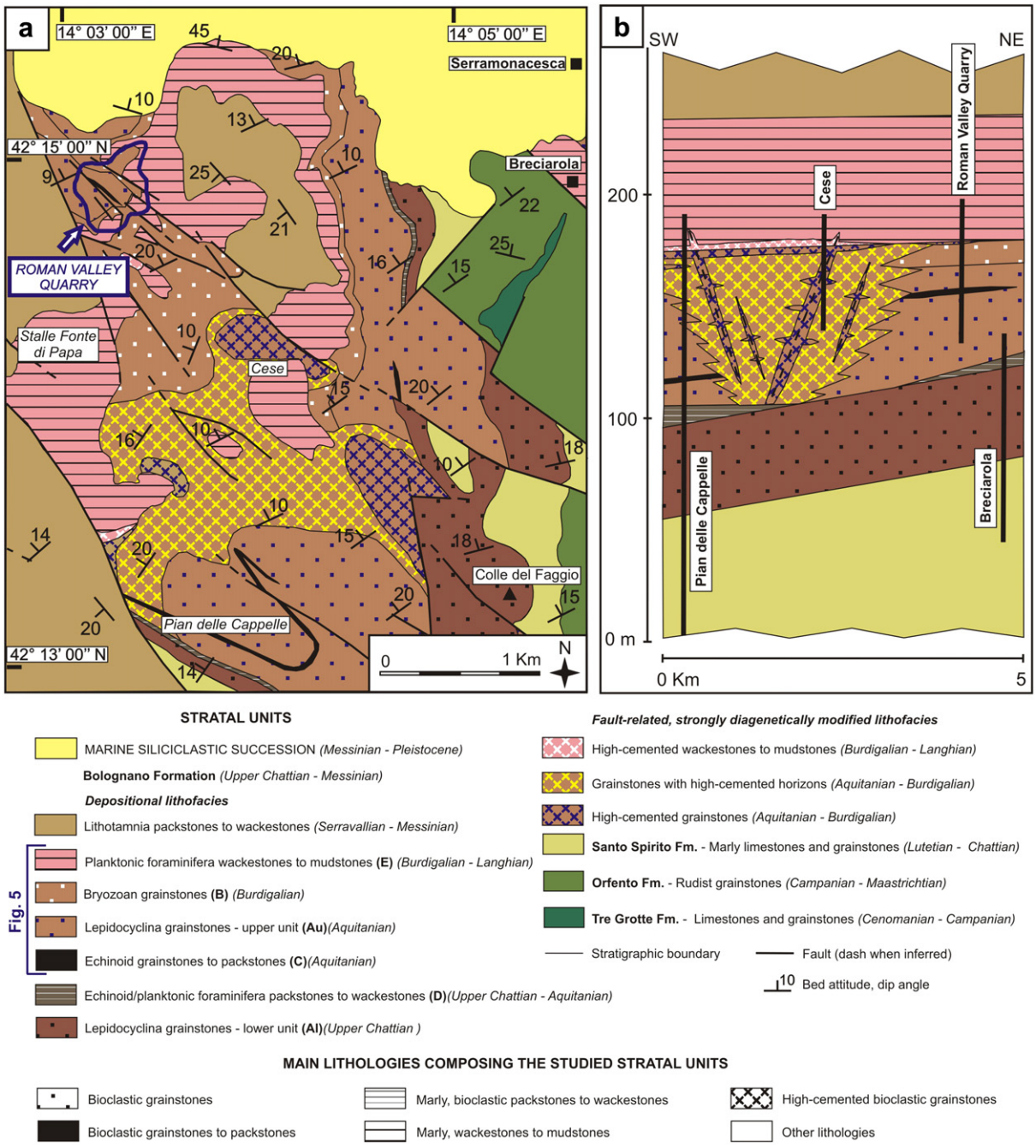

Fig. 3. Geological map (a) and statigraphic scheme (b) of the carbonates cropping out in the northern sector of Majella mountain (modified after Rustichelli, 2010).

carried out along the 100's m-long and about 80 m depth, vertical walls of the Roman Valley Quarry (Fig. 4); (iii) hand-sample collection of the structural elements and carbonate host rocks for subsequent laboratory investigation.

Petrographic thin section analysis was carried out, by using an optical polarizing microscope (Nikon Eclipse E600), to document the inner structure of the bed-parallel structural elements, as well as both texture and main components of the carbonate host rock (skeletal grains, matrix, cements and pores). Then, by means of digital image analysis of thin section microphotographs (Image-J 1.32 software), the sedimentological rock parameters (grain size, sorting, shape factor) as well as the percentage of different rock components (grains, matrix, cement, 2D porosity) were quantified. Specifically, in the following text, as a grain size we refer to the mean value of the measured diameters assuming that the individual grains are characterized by rounded shapes. Differently, sorting is expressed as an "inclusive graphic standard deviation" σi (*sensu* Folk and Ward, 1957; Flügel, 2004):

$$\sigma_i = \Phi_{84} - \Phi_{16}/4 + \Phi_{95} - \Phi_5/6,6 \quad (1)$$

where Φ represents the logarithm on base 2 of the mean grain size, according to the Wentworth – Udden scale. This parameter is compared with the chart edited by Longiaru (1987) for a qualitative classification of the carbonate rocks (e.g., well-sorted). Shape factor, instead, is expressed as the mean value of the dimensionless ratio between perimeter (P) of each individual grain and a parameter

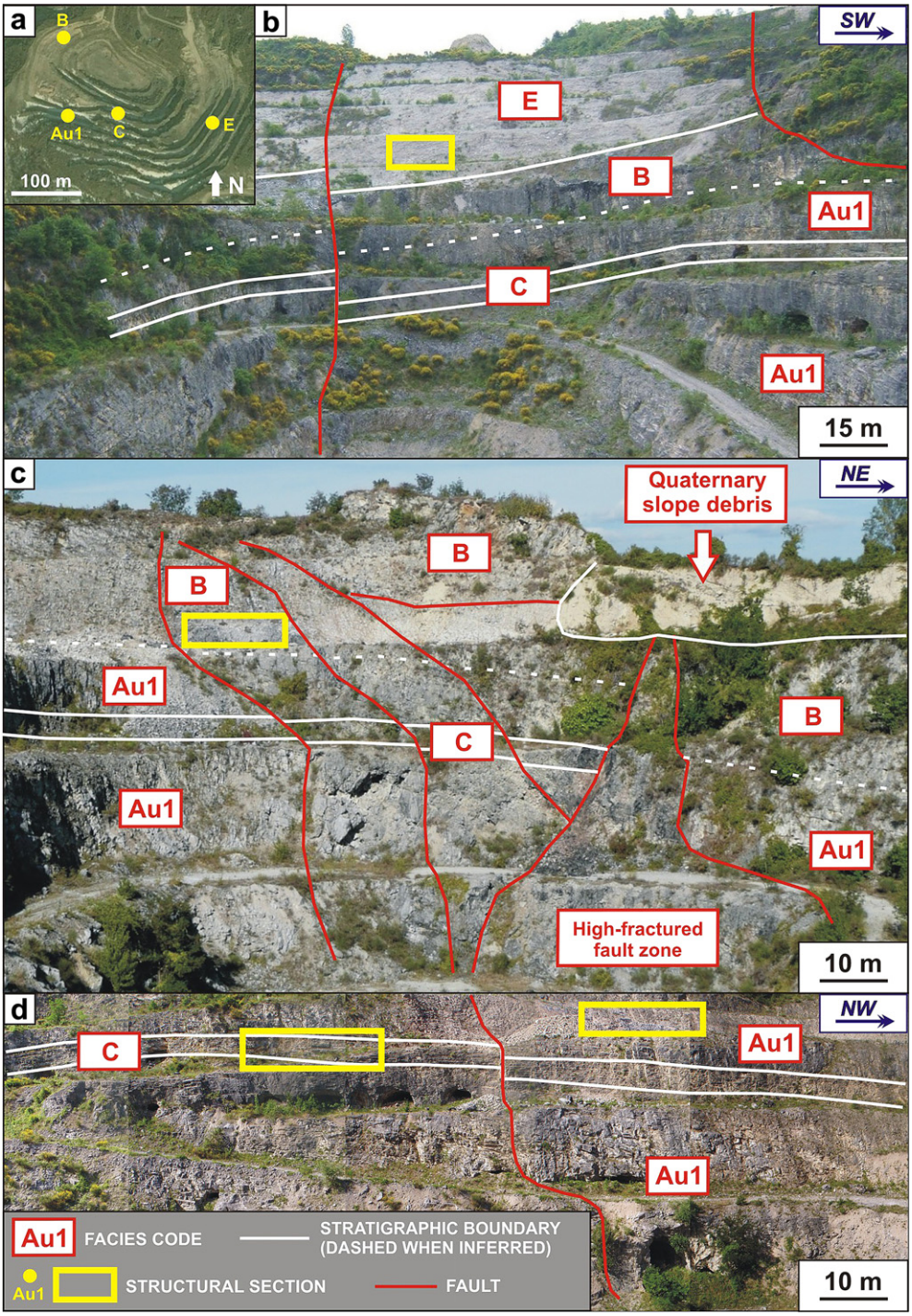

Fig. 4. a) Plant aerial view of the Roman Valley Quarry. b, c, d) Outcrop view of the three sub-vertical walls of the quarry along which the structural analysis was carried out. The most representative structural sections for each studied lithofacies/facies (see Fig. 5), are highlighted. The outcrop pictures of both Figs. 9 and 10 are referred to these structural sections.

proportional to its area ($2\sqrt{\pi A}$). The shape factor represents the grain circularity in 2D; the value of 1 is associated to a circular grain, whereas higher values are related to more elliptical grains. The percentages of the different rock components were calculated by automatic point counting, based on recognition of chromatic differences, on thin section microphotographs. In particular, this method provided 2D values of porosity, both total porosity and intergranular versus intragranular porosity. The latter porosities were recognized by mean of optical microscope analysis, which also allowed us to determine, by applying digital image analysis, sizes, shapes and distribution of macropores, which have a diameter >20 μm (Anselmetti et al., 1998).

In order to take into account also microporosity (pore diameter <20 μm), 3D connected total porosity measurements were performed by means of the Micromeritics – Multivolume Helium Pycnometer 1305. According to Anselmetti et al. (1998), microporosity can be easily calculated as the difference between 3D values (macroporosity + microporosity) and 2D ones (macroporosity).

Considering that the bulk of porosity (about 98%) is connected in all analyzed facies (Antonino Cilona, personal communication), the bulk of the measured 2D porosity can be inferred as connected and, mostly, fully comparable with 3D porosity.

Finally, HCl testing of rock powders was employed in laboratory to decipher the insoluble residue (% in volume), while X-ray diffraction analysis, carried out by mean of a KM-4 KUMA diffractometer, were aimed at inferring the rock mineralogical composition. Relationships among field and laboratory quantitative data are shown by either dispersion graphs or bar charts obtained with the "KaleidaGraph 3.5" software.

4. Host rock characterization

The carbonates pertaining to the Oligo-Miocene Bolognano Formation consist of (i) relatively shallow-water skeletal grainstones and packstones, which are made up of fragments of larger benthic foraminifera (LBF), bryozoans, red algae and lamellibranches, echinoid plates and spines, and (ii) deeper water marly wackestones and mudstones with planktonic foraminifera (Fig. 5; Vecsei and Sanders, 1999; Pomar et al., 2004; Rustichelli, 2010). These marine carbonates were deposited on an isolated, gently dipping, homoclinal carbonate ramp under tropical conditions, which were characterized by a sea water rich in nutrients (Fig. 6; Pomar et al., 2004; Westphal et al., 2010; Rustichelli, 2010). On the basis of a variety of diagnostic characteristics, namely dominant biota in the skeletal grain assemblages and depositional architectures, Rustichelli (2010) subdivided the Bolognano Fm. carbonates in 5 lithofacies (A, B, C, D, E), as reported in Table 1 and Fig. 3. Each lithofacies is comprised of several facies with specific rock texture and dominant grain size (Table 1 and Fig. 5).

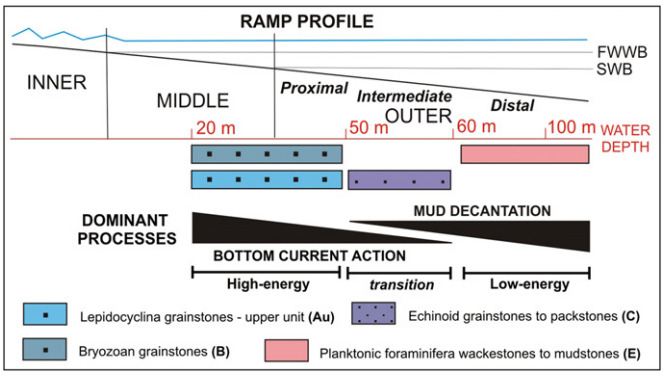

Fig. 6. Scheme showing the depositional paleoenvironments along a ramp profile, within which the studied lithofacies of the Bolognano Formation were deposited (modified after Rustichelli, 2010).

Based upon presence, distribution, and dimensional parameters (length, spacing and thickness) of the bed-parallel structural elements, six carbonate facies (Au1, B, C1, C2, E1 and E2, respectively, Tables 1, 2 and 3) were selected. The six carbonate facies, which contain different amounts of calcite and clay minerals (Table 2), cover a large range of grain size, sorting, shape, and type and amounts of skeletal grains, matrix, cements and pores (Tables 1 and 2; Figs. 7 and 8). In order to simplify our quantitative analysis, due to the similar bed-parallel structural elements they contain, E1 and E2 are conventionally considered as an individual facies, named E, hereafter in the present contribution.

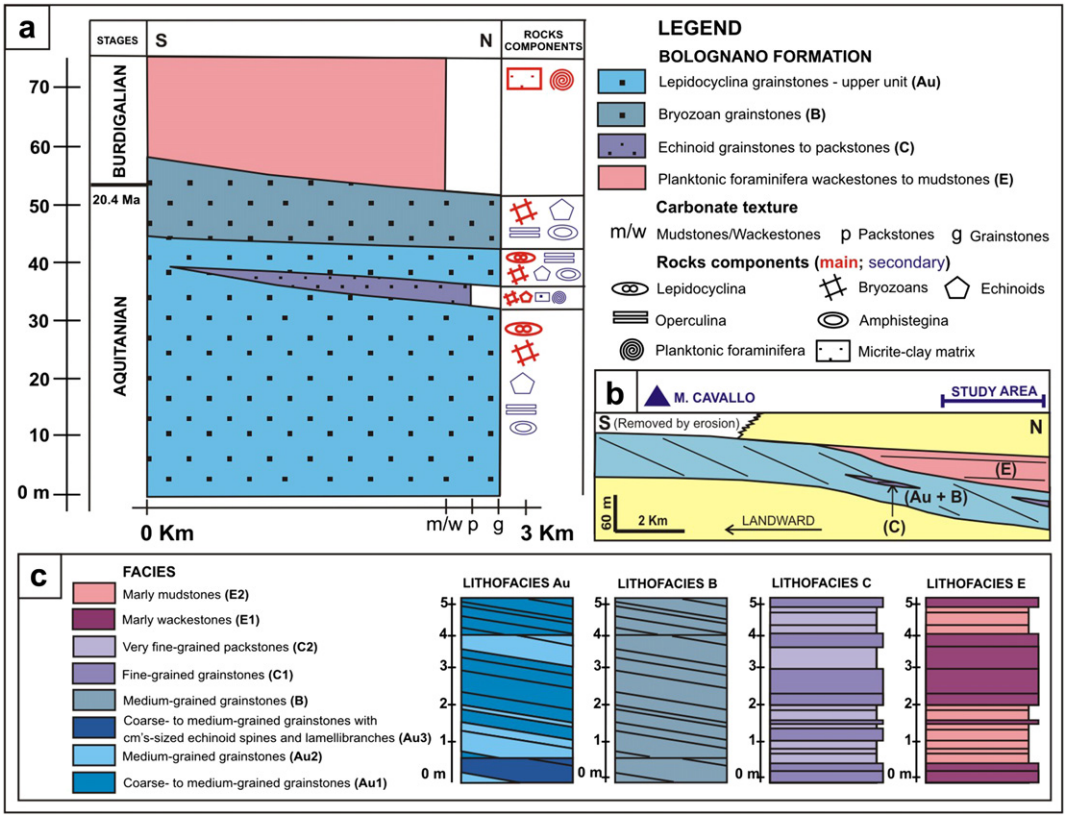

Fig. 5. a) Stratigraphic scheme of the lithofacies pertaining to the Bolognano Formation (modified after Rustichelli, 2010). b) Schematic cross section of the Majella mountain platform margin showing the large-scale architecture of the lithofacies under study (modified after Mutti et al., 1997). c) Scheme of the internal stratigraphic architecture of the studied lithofacies.

Table 1
Sedimentological, diagenetic and pore network characteristics of the carbonate facies selected for the study (highlighted in bold), in the framework of the stratigraphic units scheme proposed by Rustichelli (2010). T(m) = thickness (in meters).

Lithofacies	T (m)	Facies code	T (m)	% vol.	Lithological description	Depositional components	Depositional architecture	Diagenetic description	Pore network characteristics
A Lepidocyclina grainstones	35-40 (Al)	All	0.1-2	29	Whitish to grayish, medium − to coarse − grained bioclastic grainstones (in some cases reddish due to hydrocarbon invasion).	LBF (*Lepidocyclina, Amphistegina*, and *Operculina*), whole or as fragments, minor contents in bryozoan and red algae fragments, echinoid plates and spines.	**Stacks of dm's to up to 4 m-thick crossbed packages bounded by sub-horizontal truncation surfaces. Each package is made up of 5-80 cm-thick crossbed foresets which downlaps (normally dipping <10°) towards NNW onto the lower truncation surfaces. Individual crossbeds are sigmoidal, from 1 to 10 m-long in dip direction, and are quite planar, up to 10's m-long in strike direction. Argillaceous to marly interlayers, up to 3 cm thick, are rarely present. Individual bed packages bounded by truncation surfaces of the lithofacies A can be composed of i) alternation of 10 cm to 2 m-thick bed packages of different facies, ii) only a facies types (as for lithofacies B).**	**Moderate amounts of syntaxial overgrowth, clear calcite cement around echinoid plates and spines. Low amounts of microsparry, clear calcite cement.**	**Uniformly distributed, small specific surfaces, macropore network, which is dominated by both abundant large (0.1−0.5 mm) intergranular pores and smaller (0.05−0.2 mm) intragranular pores.**
		Al2	0.1-2	11	Whitish to yellowish, fine-grained bio clastic grainstones.				
	40-60 (Au)	**Au 1**	**0.1-2**	**28**	**Whitish to gray, medium − to coarse − grained bio clastic grainstones (commonly reddish or blackish due to hydrocarbon invasion).**	**LBF (mainly *Lepidocyclina*, minor contents in *Amphistegina* and *Operculina*, rare *Miogypsina*), whole or as fragments, minor contents in bryozoan fragments, echinoid plates and spines, Less abundant lamellibranches and red algae fragments.**			
		Au2	0.1-2	31	Whitish to gray, medium − grained bio clastic grainstones (commonly reddish or blackish due to hydrocarbon invasion).				
		Au3	2-3	1	Whitish to gray, medium − to coarse − grained bio clastic grainstones with cm-sized lamellibranches and echinoids spines (commonly reddish or blackish due to hydrocarbon invasion).				
B Bryozoan grainstones	10-15	**B**	**10-15**	**100**	**Whitish to gray, medium -grained bio clastic grainstones (commonly reddish or blackish due to hydrocarbon invasion).**	**Bryozoan fragments with minor contents in LBF (mainly *Amphistegina* and *Operculina*, rare *Miogypsina*, and sporadic, probably reworked, *Lepidocyclina*), whole or as fragments, echinoid plates and spines, red algae and lamellibranches fragments.**			

(*continued on next page*)

Table 1 (*continued*)

Lithofacies	T (m)	Facies code	T (m)	% vol.	Lithological description	Depositional components	Depositional architecture	Diagenetic description	Pore network characteristics
C Echinoid grainstones to packstones	3-5	**C1**	**0.1-1**	**52**	**Grayish to yellowish, fine – grained bio clastic grainstones.**	**Echinoid plates and spines, LBF (*Amphistegina, Lepidocyclina* and *Operculina*) and bryozoan fragments. Minor contents in planktonic foraminifera (*Globigerinoides, Globoquadrina, Catapsydrax*), lamellibranches and red algae fragments, Poorly abundant micrite-clay matrix.**	**Stacks of laterally extensive, 5-70 cm-thick planar beds. These lithofacies are composed of alternation of bed packages of different facies. The thickness of individual bed packages ranges from 10 cm to 1 m (lithofacies C), and from 10 cm to 2 m (lithofacies E). Argillaceous to marly interlayers, up to 3 cm thick, are present.**	**Abundant syntaxial overgrowth, clear calcite cement around echinoid plates and spines. Minor amounts of microsparry, clear calcite cement.**	**Patchly distributed macropore network, which is dominated by 0.05-0.15 mm large intergranular and intragranular pores.**
		C2	**0.1-1**	**48**	**Grayish to yellowish, fine – to very fine – grained bio clastic packstones.**			**Abundant microsparry, clear calcite cement. Minor amounts of syntaxial overgrowth, clear calcite cement around echinoid plates and spines.**	**Patchly distributed, high specific surfaces, macropore network, which is dominated by scattered, 0.05-0.1 mm large intragranular pores.**
D Echionoid/ planktonic foraminifera packstones to wackestones	8-10	/	/	/	Whitish to yellowish, very fine-grained bio clastic packstones to marly wackestones.	Echinoid plates and spines, LBF (*Amphistegina, Lepidocyclina* and *Operculina*) and broyozoan fragments, planktonic foraminifera (*Globigerinoides, Catapsydrax, Globoquadrina*), sponge spicules and radiolarians. Poorly abundant to dominant micrite-clay matrix.		/	/
E Planktonic foraminifera wackestones to mudstones	60-65	**E1**	**0.1-2**	**55**	**Grayish, marly wackestones.**	**Planktonic foraminifera (e.g., *Praeorbulina* and *Orbulina*), minor radiolarian and sponge spicules. Dominant micrite-clay matrix.**		**Moderate amounts of microsparry, clear calcite cement, within internal chambers of planktonic foraminifera.**	**Uniformly distributed, intra-matrix micropore network with scattered intragranular macropores, 0.05-0.1 mm large with low specific surfaces.**
		E2	**0.1-2**	**45**	**Grayish, marly mudstones.**				

Table 2
Sedimentological, compositional and pore network parameters of the carbonate facies considered in this study (mean values and ranges from 8 samples for each facies; solely for the 3D total porosity are considered 3 samples for each facies). Legend: GS = grain size (mm); S = sorting (vw = very well; w = well; m = moderate; p = poorly); SF = shape factor; Ca = calcite (% vol.); IR = insoluble residue, composed of clay minerals (% vol.). Rock components (% vol.): G = grains; M = matrix; Lp = *Lepidocyclina*; Bz = bryozoans; Ec = echinoids; PF = planktonic foraminifera; C = cement; (2D)Pt = 2D total porosity; (2D)Pì = 2D intergranular porosity; (2D)Pìì = 2D intragranular porosity; 3D(Pt) = 3D total porosity. Empty cells = incalculable values.

Facies code		GS	S	SF	Ca	IR	G	M	Lp	Bz	Ec	PF	C	(2D)Pt	(2D)Pi	(2D)Pii	(3D)Pt
Au1	Mean value	0.52	0.92 (m/p)	1.31	99.5	0.5	79.3	0	51.6	20.1	5.2	0	4.1	16.6	10.8	5.8	23.9
	Range	0.23–0.62	0.8–1.06	1.23–1.35	99.3–99.7	0.3–0.7			42.5–71.4	11.8–27.7	4–11.2		3–6.3	10.4–25.9	7–19.1	3.9–7.1	15.3–33.2
B	Mean value	0.3	0.6 (m/w)	1.22	99.5	0.5	70	0	0.5	44.1	12.8	0	4.5	24.6	19.4	5.2	32.1
	Range	0.18–0.35	0.48–0.69	1.18–1.26	99.3–99.7	0.3–0.7			0–1	37.9–68.8	8.9–16.5		3–7.2	21.2–28.6	16–22.5	3.8–8.3	26.4–35.3
C1	Mean value	0.15	0.54 (w/m)	1.15	98.9	1.1	82	4	0	0	25.5	3.5	7.5	6.5	3.9	2.6	10.2
	Range	0.14–019	0.47–0.62	1.14–1.17	98.2–99.5	0.5–1.8	79.3–87.5	0–7.5			19.4–31.2	0.5–6.1	4.5–10.4	4.2–8.7	2.8–5.2	2–4.1	5.8–14
C2	Mean value	0.14	0.37 (w/vw)	1.15	97.2	2.8	74.7	16	0	0	20.1	7.8	8.8	0.5	0	0.5	3.9
	Range	0.12–0.15	0.33–0.42	1.14–1.16	96–98.1	1.9–4	70.2–83.1	7.5–22			12.6–25.9	4.1–10.2	6–11.9	0.1–2.1		0.1–2.1	1.4–7.2
E	Mean value				89.7	10.3	12.1	85	0	0	0	11.1	1.8	1.1	0	1.1	29.9
	Range				82.2–94.8	5.2–17.8	2.9–31.2	65–95				3.3–22.4	0.8–4.4	0.4–2.1		0.4–2.1	24.9–33.1

Table 3
Dimensional parameters (mean values and ranges from 30 measures per bed-parallel structure type in each facies) of the bed-parallel compaction bands (CB) and pressure solution seams (PSS) localized within individual carbonate beds, analyzed in this study. "PSS thickness" is the thickness of the clayish insoluble material associated to the PSS.

Facies code		CB length (cm)	CB spacing (cm)	CB thickness (mm)	Pattern	PSS length (cm)	PSS spacing (cm)	PSS thickness (mm)	Pattern
Au1	Mean value	3	38	1	Isolated	15.6	36.7	0.5	Isolated
	Range	0.9–8.7	10.2–80.4	0.5–3.2		2.6–36.7	10.1–146.2	0.1–2	
B	Mean value	10	20	2.5	Isolated	17.5	29.7	0.6	Isolated
	Range	2.4–23.8	6.1–82.2	0.5–5		3.1–33.4	12.1–82	0.1–2.1	
C1	Mean value					28.8	8.5	1	Isolated
	Range					5.6–56.3	0–29.9	0.2–3.5	
C2	Mean value					84.8	2.4	1.6	Anastomosed
	Range					2.4–167	0–5.6	0.4–8.2	
E	Mean value					28.7	17	0.8	Isolated
	Range					2.7–50.5	7.7–34	0.2–2.3	

5. Structural analysis

The structural elements object of this study consist of one set of deformation bands and one set of pressure solution seams both oriented sub-parallel to bedding (Figs. 9 and 10). Bedding, deformation bands and pressure solution seams are all dipping 10–15° toward north (Fig. 11a). The two sets of bed-parallel structures represent the first elements that developed within the studied carbonates (Agosta et al., 2009). Both deformation bands and pressure solution seams, in fact, pre-date all bed-perpendicular

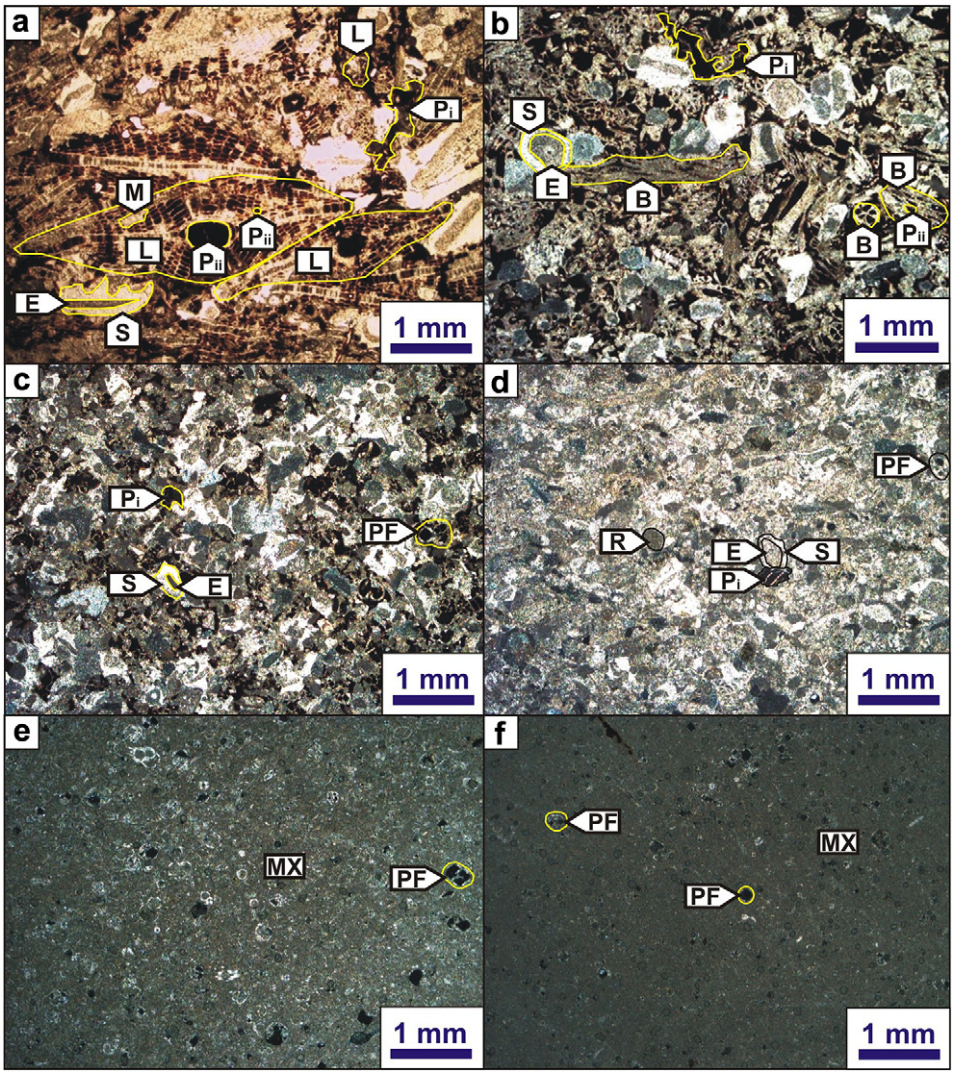

Fig. 7. Studied facies under a cross-nicols optical microscope view. a) *Lepidocyclina*-dominated, skeletal grainstones of facies Au1. b) Bryozoan-dominated, skeletal grainstones of the facies B. c) Fine-grained grainstones of the facies C1. d) Fine- to very fine-grained packstones of the facies C2. e) Marly wackestones of the facies E1. f) Marly mudstones of the facies E2. Legend: *Lepidocyclina* (L), bryozoan fragment (B), *Amphistegina* (A), planktonic foraminifera (PF), echinoid plate (E), red algae (R), matrix (MX), syntaxial overgrowth (S) and microsparry (M) cements, intergranular (Pi) and intragranular (Pii) porosities. Note the intragranular porosity (black) internal to the highlighted planktonic foraminifera in c), d), e) and f).

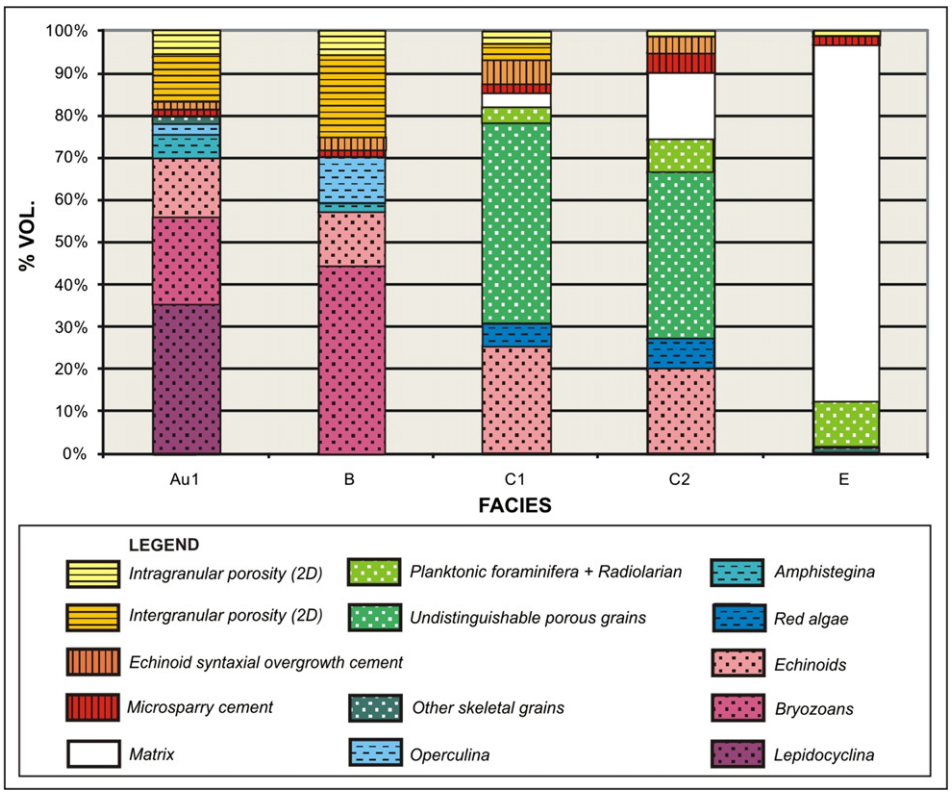

Fig. 8. Bar chart showing the relative mean amounts of the rock components (i.e., skeletal grains, matrix, cements and pores) for the different facies of the Bolognano Formation (modified after Rustichelli, 2010).

and bed-oblique fractures, compactive shear bands, and both bed-bounded and through going slip surfaces (Figs. 9 and 10).

In the field, the bed-parallel deformation bands appear lightly colored with respect to the surrounding host rock (i.e. grainstones) which, in many cases, is black in color due to hydrocarbon invasion. No evidence of shearing was found across deformation bands. These structural elements form narrow bands localized either at the bed interfaces (Fig. 9a) or, alternatively, within individual

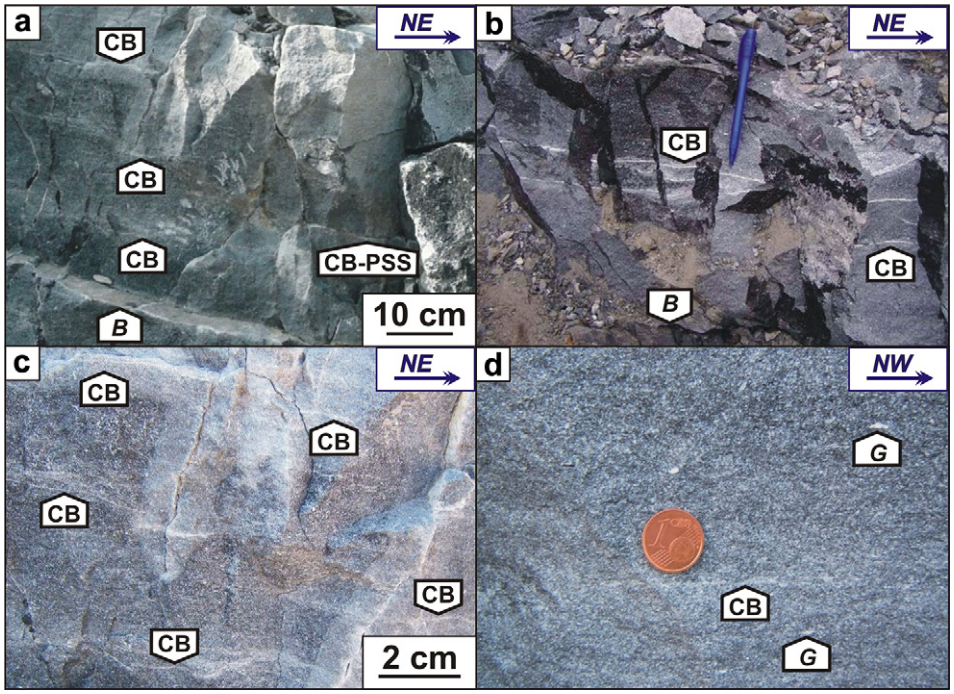

Fig. 9. Compaction bands (CB) parallel to bedding (*B*) analyzed along the sub-vertical walls of the Roman Valley Quarry. a-b-c) CB affecting the grainstones of the facies B. Pen is for scale. The grainstones (blackish) are strongly invaded by hydrocarbons that highlights the CB (whitish). d) One of the longest CB, localized within an individual carbonate bed, affecting the grainstones of the facies Au1. Coin is for scale.

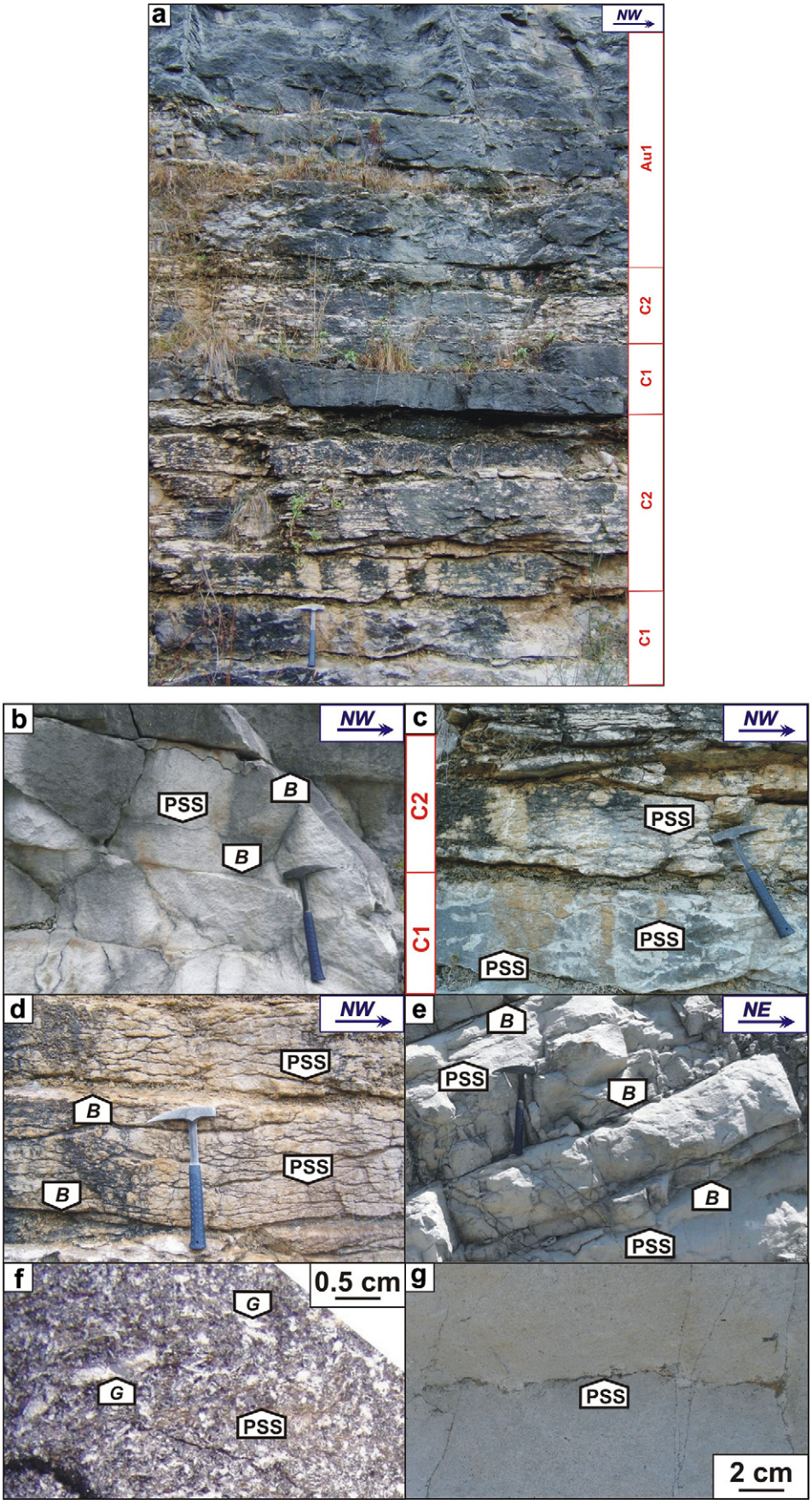

Fig. 10. Pressure solution seams (PSS) parallel to bedding (*B*) analyzed along the sub-vertical walls of the Roman Valley Quarry. Distribution of PSS in the facies Au1 (a and b), C1 (a and c), C2 (a and d) and E (e). Hammer is for scale. f) Isolated PSS, marked by reddish residue material, localized within an individual carbonate bed of the facies Au1. Note that PSS is sub-parallel to elongated grains (*G*), which have the long axis iso-oriented relative to bedding. g) Isolated PSS localized within an individual carbonate bed of the facies E.

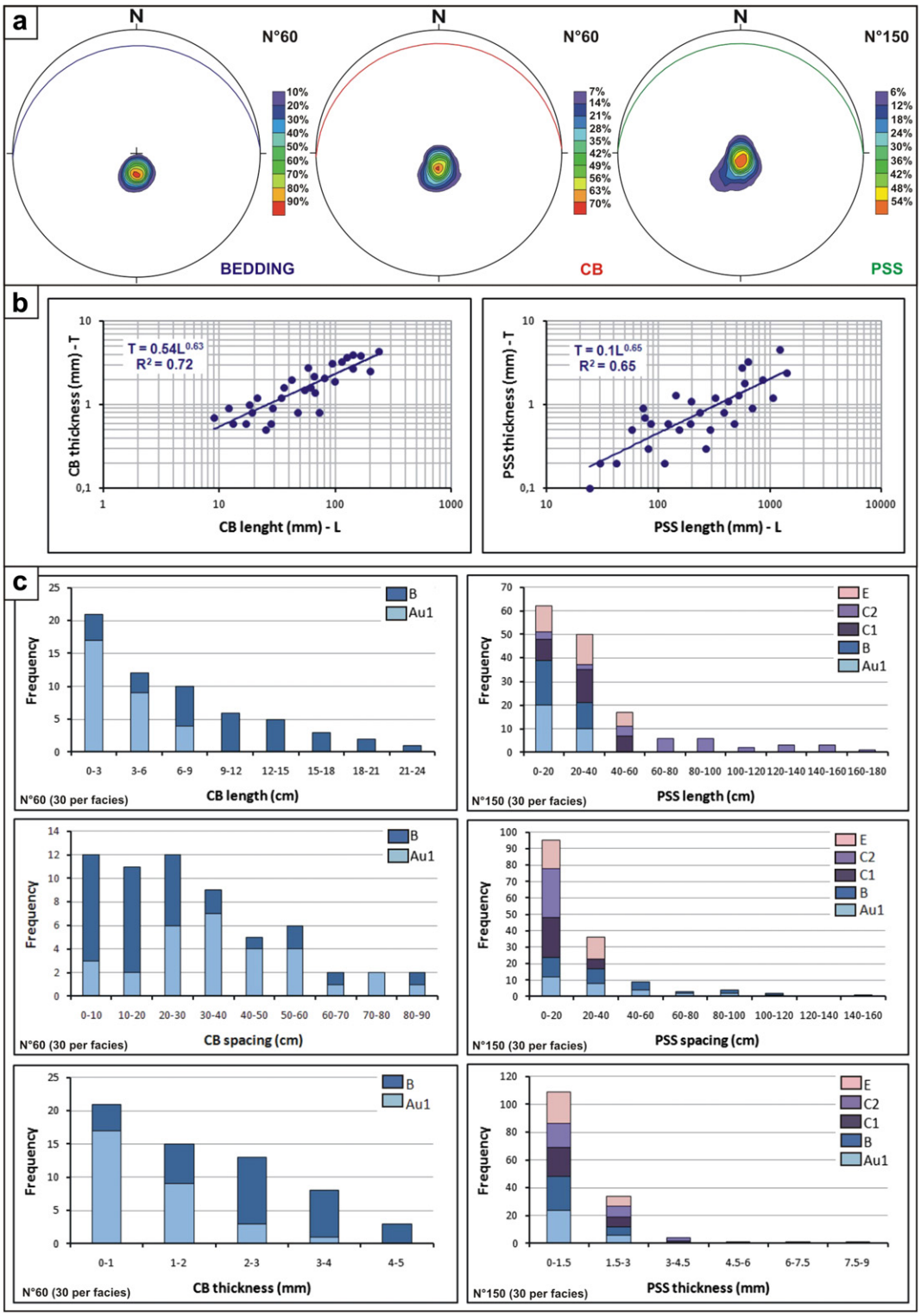

Fig. 11. a) Contour plots (with associated mean cyclographs) of poles of the planar elements (i.e. bedding, compaction bands, CB, and pressure solution seams, PSS, localized within individual carbonate beds) documented in the host rock. Stereographic projection, lower hemisphere. b) Dispersion graphs showing the best-fitting quantitative correlations (power-law) between length and thickness of either CB or PSS. c) Bar charts showing the (i) length, (ii) spacing and (iii) thickness of either CB or PSS versus frequency for each of the studied facies.

carbonate beds (Figs. 9b, c and d). In the latter configuration, the bands consist of individual straight-to-wavy structures, up to 25 cm-long, and 0.5 to 5 mm-thick (Figs. 9, 11b and c). In many cases, the longest bands also represent the thickest ones (Fig. 11b). Less commonly, zones of sub-parallel bands, spaced less than 1 m, are present (Fig. 9b). All the deformation bands are oriented sub-parallel to the long axes of the grains composing the rock (*G*, in Fig. 9d) which are, in turn, iso-oriented relative to bedding.

Under the optical microscope, the inner texture of the bands consists of tight grains with very little amount of 2D porosity

(commonly 0–5%). Typically, the long axis of the individual grains internal to the bands is parallel to these (Fig. 12a), which is consistent with their rotation during compaction. The individual bands are separated by the surrounding host rock by two outer, transitional zones, not visible at an outcrop scale. Individual transitional zones, commonly thick from 1/2 to 1/5 of the adjacent bands, are made up of less tight grains and higher amount of 2D porosity (in the order of a few percent; Fig. 12a). From the external to the internal zones of the bands, a progressive grain size reduction was, in some cases, observed along the thickest bands (Fig. 12a). This determines a change from coarse – to medium sand grain sizes, of the host rock, to fine sand-to-mud (<0.025 mm) grain sizes of the internal zones of the bands (Fig. 12a). An increased number of fractured grains (commonly <30%), furthermore, is associated to the zones of reduced grain size (Fig. 12a and b). Immediately adjacent to individual bands, and within them, a very few grains show calcite twinning, as reported by previous works (Ferrill and Groshong Jr., 1993; Vajdova et al., 2010). Sutured grain-to-grain contacts (Fig. 12a and b) are observed in the thickest bands. These sutured contacts mainly affect grains characterized by minimal internal pores (echinoids). The thickest bands may also contain microsparry cements infilling both primary and secondary porosity (mode I fractures). These cements can decrease the porosity even further in some bands relative to the surrounding host rock (Fig. 12a and b). As a consequence of the progressive packing of the grains from the external transitional zones to the inner portion of the individual bands and lack of clear evidence of shearing, these structural elements are classified as compaction bands (CB).

At an outcrop scale, the bed-parallel pressure solution seams (PSS) are characterized by a columnar to wavy form (Fig. 10) and, commonly, show a negative relief with respect to the host rock due to erosion along the weaker, mm-thick clayish material marking the structure (Fig. 10f and g). PSS localize either at the contacts between adjacent beds and/or within individual beds. In a few cases, PSS are present within individual bed-parallel compaction bands (CB-PSS in Fig. 8a; Fig. 12a). Locally, PSS at contacts between adjacent beds show striation and, therefore, evidence of shearing. PSS within individual beds are long up to 1.7 m (Fig. 11c), and commonly form isolated structural elements (Fig. 10b and e); in a few cases, they are arranged with anastomosed patterns (Fig. 10c and d). Spacing of PSS present within individual beds varies from <1 cm to a few 10's of cm (Fig. 11c).

At a microscope scale, PSS appear as 10's μm to mm-thick seams made up of reddish clayish material (Fig. 12c, d, f, g). Within the thickest, mm-thick seams present in the skeletal grainstones, the undissolved grains, mainly echinoid fragments, show evidence of size reduction due to fracturing (sizes from fine sand to silt). These tiny undissolved grains are enveloped within a reddish clayish matrix, and display sutured grain-to-grain contacts (Fig. 12c and d). Differently from CB, PSS contained in grainstones are characterized by a sharp 2D porosity reduction (down to 0–5%) and absence of any microsparry cements (Fig. 12c and d). Clear evidence of pervasive intergranular dissolution (sutured grain-to-grain contacts) are present, primarily, at the contact points between adjacent skeletal grains (mainly echinoids and red algae) characterized by lack of internal porosity (Fig. 12d and f).

6. Correlation among compositional, sedimentological and structural parameters

In order to avoid any effect due to (i) presence of sedimentary structures such as bed interfaces and (ii) possible shearing during bed tilting (Agosta et al., 2009), in the present contribution only bed-parallel compaction bands (CB) and pressure solution seams (PSS) localized within individual carbonate beds are considered (Fig. 10). Hereafter, in fact, the correlations among compositional, sedimentological and pore network characteristics of carbonate rocks (Table 2) and both spacing and length of the studied bed-parallel structural elements, will be assessed.

CB are present only within the medium- to coarse-grained grainstones of facies Au1 (mean grain size comprised between 0.23 and 0.62 mm) and the medium-grained grainstones of facies B (mean grain size comprised between 0.18 and 0.35 mm). In the two facies, however, CB are characterized by different length, spacing and thickness (Fig. 9). Individual CB are, in fact, longer, less-spaced and thicker within facies B than in Au1 (Table 3 and Fig. 11c).

Even though PSS are present within all the studied carbonates, they show significant differences with respect to their dimensional parameters and patterns among the different facies (Table 3 and Fig. 10). In particular, the length of individual PSS is up 1.7 m in the fine- to very fine-grained packstones of facies C2 (mean grain size comprised between 0.12 and 0.15 mm), in which PSS show the lowest spacing values, the highest thickness of clayish residue material and a peculiar anastomosed pattern (Table 3, Figs. 10d and 11c). Microscope observations are consistent with these packstones being characterized by the most pervasive intergranular pressure solution evidence (sutured grain-to-grain contacts) among the studied carbonates (Fig. 12f).

The most meaningful quantitative correlations, documented among the various compositional, sedimentological, pore network and structural parameters of the studied carbonate rocks, are shown in Figs. 13 and 14. The individual data points displayed in the correlation graphs represent the mean value for each studied carbonate facies (see Tables 2 and 3).

As reported above, CB are exclusive of grainstones characterized by mean 2D and 3D values of total porosity higher than about 10 and 15%, respectively (facies Au1 and B). CB are longer and closely spaced in the facies B, which is characterized by the highest 2D and 3D mean values of porosity (Fig. 13). Conversely, as shown in the correlation graphs of Fig. 14, the individual PSS show the highest mean values of lengths, as well as the lowest mean values of spacing, within the fine- to very fine-grained packstones of facies C2. These carbonate rocks containing a specific range of clayish insoluble residue (2–4% in volume, in which the most prevalent mineral is illite; Fig. 14a). The mean spacing of PSS is positively correlated to the mean grain size, grain sorting and shape factor, while their mean lengths are negatively correlated to the aforementioned sedimentological parameters (Figs. 14b, c and d).

7. Discussion

Similar to what it has been previously documented for bed-parallel compaction bands (CB) by Tondi et al. (2006), thin section observations suggest that physical compaction of grainstones determined progressive strain localization and porosity reduction within narrow, mm-thick tabular bands (Fig. 12a). This process has also been observed in limestone samples characterized by a wide range of 3D porosity (3–37%) deformed in the laboratory under triaxial loadings (Baud et al., 2000, 2009; Vajdova et al., 2004; Zhu et al., 2010; Vajdova et al., 2010). The aforementioned studies addressed a mechanism of inelastic compaction and cataclastic flow, which was characterized by pore collapse and in some cases, grain crushing (Vajdova et al., in press). For the first time, in this article the contribution of intergranular pressure solution and subsequent cement precipitation to compaction and porosity reduction in the internal zone of CB is reported. In fact, in correspondence of the thickest CB it is possible to note that intergranular pressure solution is accompanied by extensive precipitation *in situ* of syn-compactional microsparry cements infilling the intra-grain,

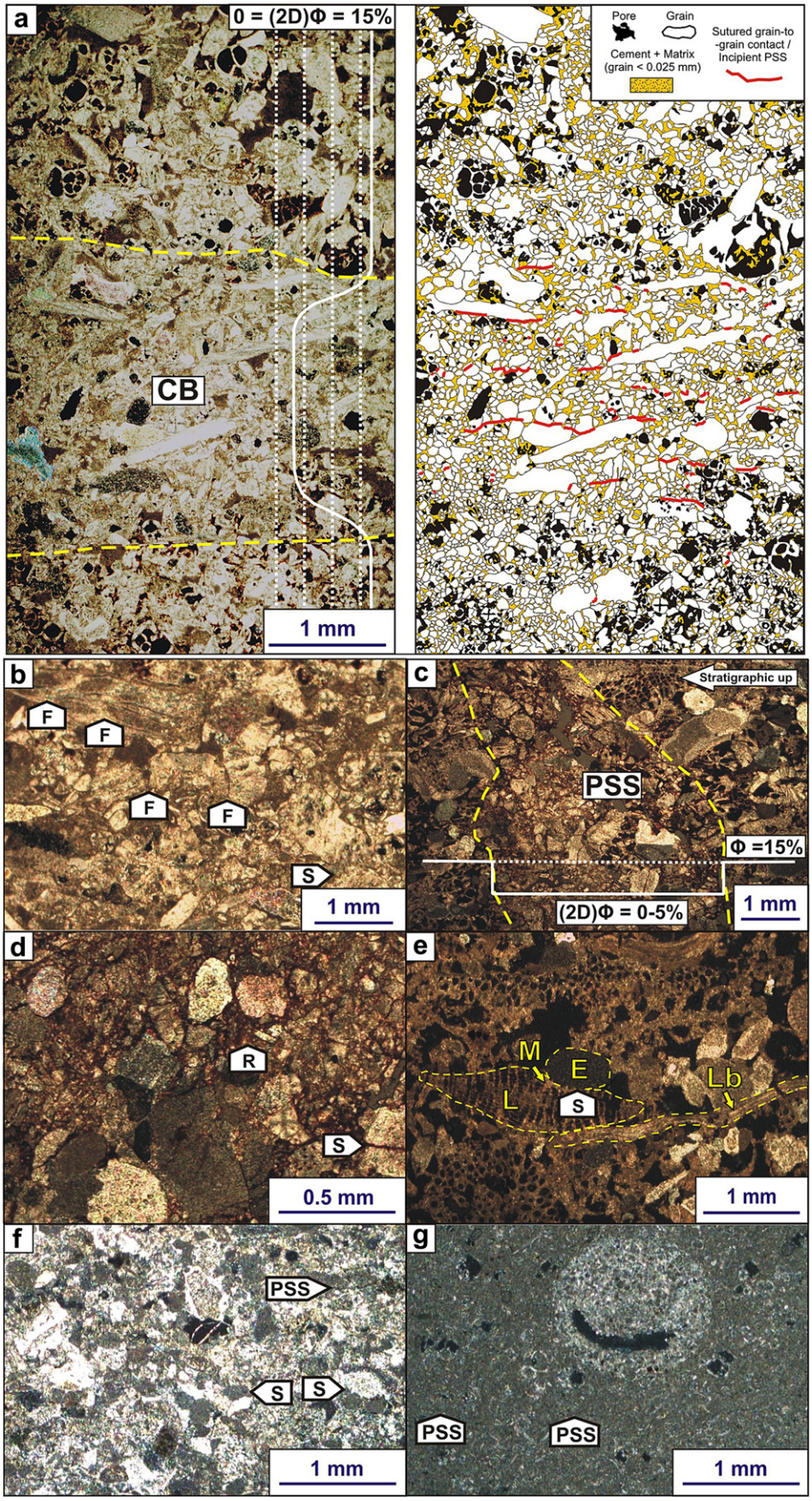
a
0 = (2D)Φ = 15%
CB
1 mm
Pore
Grain
Cement + Matrix
(grain < 0.025 mm)
Sutured grain-to
-grain contact /
Incipient PSS
b
F
F
F
F
S
1 mm
c
Stratigraphic up
PSS
Φ =15%
(2D)Φ = 0-5%
1 mm
d
R
S
0.5 mm
e
M
E
L
S
Lb
1 mm
f
PSS
S
S
1 mm
g
PSS
PSS
1 mm

mode I fractures (Fig. 12a and b). Thin section observations show precipitation of microsparry cements which are coeval to intergranular pressure solution; these cements represent the re-precipitation of dissolved calcite at skeletal grain-to-grain contacts (Fig. 12e, cf. Rustichelli, 2010). The fact that, within the bands, pressure solution processes post-date grain fracturing and inelastic compaction is analogous to what it has been previously documented for compactive shear bands (Tondi et al., 2006; Tondi, 2007).

Field observations show that the individual CB grew in length and thickness at the same time. The longest structures, in fact, correspond to the thickest ones (Fig. 11b). The power–law correlation between CB length and thickness (Fig. 11b), characterized by an exponent = 0.63, is quite similar to that documented by Tembe et al. (2008) and Schultz (2009) for compaction bands in sandstones.

The results of field and, mainly, thin section analyses are consistent with intergranular pressure solution determining the development of localized bed-parallel pressure solution seams (PSS), in agreement with numerous previous studies (Bathurst, 1958; Weyl, 1959; Petit and Mattauer, 1995; Renard et al., 2004). Both intergranular pressure solution evidence in form of suturated grain-to-grain contacts (Fig. 12e), and localized 10's μm thick, isolated PSS were observed (Fig. 12f and g). In order to explain the data, it is invoked a process consistent with the propagation of individual PSS perpendicular to the maximum, compressive principle stress axis, due to intergranular pressure solution accelerated by stress concentration around the PSS tips, similar to what it has been proposed for anticrack model (Fletcher and Pollard, 1981). The lateral propagation of individual PSS was accompanied by continuous formation of clayish insoluble material, which probably became progressively thicker, from 100's μm to mm, during ongoing deformation (Figs. 10b, e, f, g) enveloping undissolved, strongly fractured and size-reduced grains (Fig. 12c and d). Along this line, the development of closely spaced anastomosed PSS by merging of isolated elements is inferred to have occurred during advanced stages of deformation (Fig. 10d).

In the next chapters, the role of compositional, sedimentological and pore network characteristics of the carbonates on the development and distribution of the studied bed-parallel structural elements is discussed by assuming similar boundary conditions (burial depth: 200–2500 m; pressure: 4–60 MPa; Ori et al., 1986; Mutti, 1995).

7.1. Controls of rock characteristics on development of bed-parallel compaction bands

Among the studied carbonate facies, the bed-parallel compaction bands (CB) are present only within medium- and medium- to coarse-grained grainstones. These rocks are characterized by 2D and 3D values of porosity comprised between 10 and 29%, 15 and 35%, respectively (Table 2 and Fig. 13). Our observations show that CB are more developed within the medium-grained grainstones of facies B (25% of mean 2D total porosity, 19% of mean 2D intergranular porosity) than in the medium- to coarse-grained grainstones of facies Au1 (17% of mean 2D total porosity, 11% of mean 2D intergranular porosity), and suggest that CB formation was strongly dependent on porosity (Baud et al., 2004; Tondi et al., 2006). Moreover, the aforementioned empirical relationships highlight the control exerted by porosity type and distribution on compaction banding. A high amount of uniformly distributed, well-connected intergranular macroporosity strongly enhanced CB formation because, probably, it facilitated the process of pore collapse by mean of grain translation and rotation. On the contrary, the empirical relationships indicate that the amount of intragranular macroporosity did not influence compaction banding. Similar values of intragranular macroporosity (5–6%) were, in fact, found for facies B and Au1, which are characterized by dissimilar distribution of CB (see Tables 2 and 3, and Fig. 11c).

The different control exerted by macroporosity relative to microporosity on CB development can be also inferred taking into account that, despite being characterized by 3D porosity values similar to those of facies Au1 and B, the wackestones and mudstones of facies E do not contain any CB (Table 2 and Fig. 13b). Both facies Au1 and B are dominated by macroporosity, whereas facies E by microporosity. This positive relationship between amount of macroporosity and CB development is in agreement with recent works on deformation banding in carbonates. Rath et al. (2011), in fact, documented that natural deformation bands have a reduced macroporosity relative to the host rock but a preserved inner microporosity. Zhu et al. (2010) by mean of detailed microstructural observations, showed that micropores are relatively pressure-insensitive in comparison to macropores.

Differently from what previously suggested by Tondi et al. (2006), who observed compaction bands mainly within coarse-grained carbonates, the results of this study suggest that finer-grained, and better sorted grainstones with spherical grains are keen to compaction banding (Fig. 11c). Moreover, it was observed that large and elongated grains may represent mechanical obstacles to pore collapse and, hence, compaction banding (Fig. 12b).

The results of our qualitative and quantitative analyses indicate that both grain sorting and sphericity have a more pronounced effect on compaction banding than the mean grain size. Specifically, rocks with bryozoans as the dominant skeletal grain type are better sorted and are characterized by more spherical grains than those rich in *Lepidocyclina*. The former carbonate grainstones have higher values of homogeneously distributed, and well-connected, intergranular macroporosity (Table 2, Fig. 7a and b), and, hence, are more affected by compaction banding. That homogeneous porous media enhance CB development was also proposed by Louis et al. (2007).

The results of the present study also suggest that a high amount of cement is key in order to prevent CB formation in fine-grained grainstones (facies C1), especially, and fine- to very fine-grained packstones (facies C2). According to Rustichelli (2010), these rocks were affected by pre-compactional cementation, which mainly consisted of syntaxial overgrowth cement around echinoid plates and spines (Table 1, Fig. 7); and syn-compactional cementation during coeval, burial-related, pressure solution with precipitation of microsparry cement (Table 1, Fig. 7). Taking into account that the physical compaction of sediments pre-dated pressure solution, only the syntaxial overgrowth cement could have affected compaction banding. Within coarse- to medium-grained and medium-grained grainstones (facies Au1 and B), syntaxial overgrowth cement is scarce in volume (1–4%) and localizes around isolated echinoid plates and spines (Fig. 7a and b). Differently, in the fine-grained grainstones (facies C1, Fig. 7c), the tight

Fig. 12. Bed-parallel compaction bands (CB) and pressure solution seams (PSS) under an optical microscope view. a) CB within the facies B. c) Detail of the internal zone of a CB present within the facies B. Note the extensive presence of microsparry cement. c-d) PSS within the facies Au1. e) Evidence of intergranular pressure solution in facies Au1. Note the microsparry cement precipitated into plastically deformed *Lepidocyclina* internal pores, nearby the suturated contact with an echinoid plate. f) Evidence of pervasive intergranular pressure solution within facies C2. Intergranular pressure solution mainly focused on echinoid plates and associated syntaxial overgrowth cements (light "grains"), and red algae (dark grains). g) Incipient PSS within the facies E. Legend: (F) = fracture; (S) = suturated grain-to-grain contact; (R) = reddish residue matrix; (E) = echinoid plate; (M) = microsparry cement; (L) = *Lepidocyclina*; (Lb) = lamellibranch.

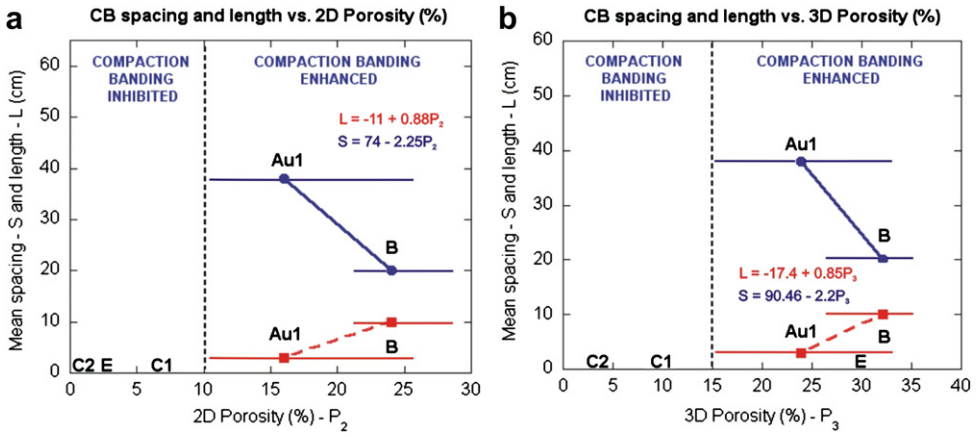

Fig. 13. The graph shows the best-fitting quantitative correlations between host rock porosity (2D and 3D), and spacing (circles) and length (squares) of bed-parallel compaction bands (CB) localized within individual carbonate beds. In both graphs, the horizontal bars adjacent to each point represent the ranges of porosity (see Table 2). In b, CB development is inhibited in facies E despite its high 3D porosity (mean value about 30%). This is due to the predominance of microporosity (about 29%), which is quite unable to promote compaction banding.

framework formed by this pre-compactional cement (up to >10% in volume) may have inhibited grain rotation and translation and, hence, CB development.

The documented role of cement in CB development could be the main reason because CB have not been observed in laboratory deformed samples of limestones, with the exception of the case study presented in the recent article of Cilona et al. (submitted for publication). The carbonates studied so far in the laboratory, in fact, were for practical reasons relatively well cemented and, so, not prone to develop CB.

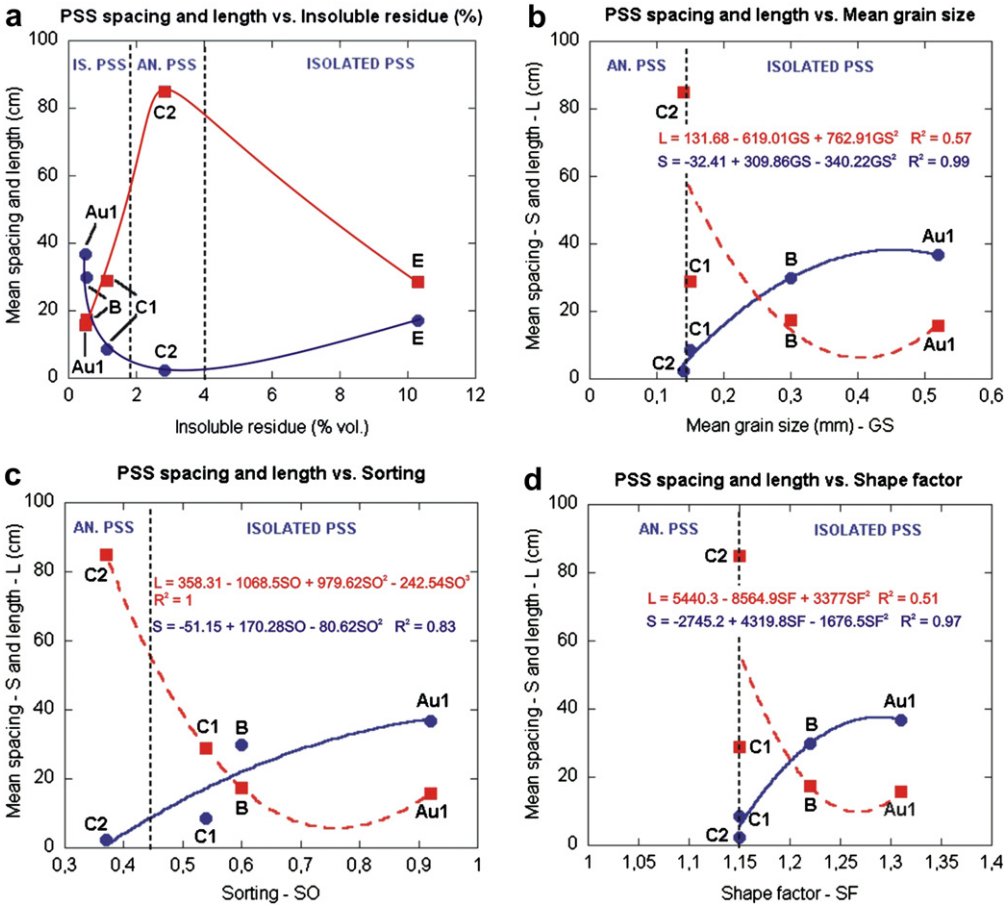

Fig. 14. The graphs show the best-fitting quantitative correlations between host rock parameters and spacing (circles) and length (squares) of bed-parallel pressure solution seams (PSS) localized within individual carbonate beds. Facies E is not considered in b, c and d. In a, the correlation curve cannot be expressed as a simple equation. Legend: IS. PSS = isolated pressure solution seams; AN. PSS = anastomosed pressure solution seams.

7.2. Controls of rock characteristics on development of bed-parallel pressure solution seams

Although bed-parallel pressure solution seams (PSS) are present in all studied carbonate facies, they are characterized by different dimensional parameters (Table 3). Bed-parallel PSS are mostly developed within the fine- to very fine-grained packstones of facies C2, in which they denote a peculiar anastomosed pattern. Due to the small amounts of clay (2–4% in vol.) in those rocks, it is possible to infer that it might have enhanced pressure solution (Fig. 14a). The role of clay minerals in pressure solution has been widely debated in the past; several experimental studies, conducted on different types of sedimentary rocks (carbonates, sandstones and halite), documented that small amounts of clay in rocks (at least 1–2% in volume) may increase dissolution (Weyl, 1959; Andrews and Railsback, 1997; Renard et al., 1997, 2001; Aharonov and Katsman, 2009).

The results of the present study are consistent with the PSS being more developed in carbonates with specific grain sedimentological parameters: (i) fine grain sizes, (ii) good grain sorting and (iii) high grain sphericity (Figs. 14b, c and d) typical of the packstones of facies C2. These results are in agreement with previously published works, which show that fine-grained carbonate rocks are more prone to pressure solution than coarser-grained ones (Weyl, 1959; Schmoker and Halley, 1982; Halley and Schmoker, 1983; Heydari, 2000). The former rocks promote material removal and transport by diffusion in the pore fluid phase, and, therefore, dissolution rates. The good sorting and sphericity of grains imply a greater number of grain contacts and, hence, stress concentration sites relative to a rock with similar composition and grain size and poorer grain sorting and sphericity (Passchier and Trouw, 1996).

Furthermore, our microscope observations suggest that intergranular pressure solution, mainly, localized at the contact points of grains characterized by absence of internal pores (mainly echinoids and red algae), which dominate the grain assemblage of facies C2 (Fig. 12f). Skeletal grain assemblage of rock is, hence, inferred as a controlling factor on pressure solution. Facies C2 is also characterized by the highest amount of cement among the studied carbonates (Table 2). Even if some authors documented that pre-existing cements may prevent intergranular pressure solution (Sibley and Blatt, 1976; Tada and Siever, 1989), thin section observations are consistent with intergranular pressure solution being focused, in many cases, at the boundaries between the pre-compactional, syntaxial overgrowth cements and skeletal grains (Fig. 12f). The pre-compactional cement framework, probably, hold together the grains during the bulk overburden, preventing them to accommodate strain by mean of physical compaction processes. High amounts of pre-compactional cements may have therefore enhanced the pervasive distribution of PSS within facies C2.

Another peculiarity of the rocks pertaining to facies C2 is their low 2D and 3D values of total porosity (see Table 2). However, Merino et al. (1983) documented that the development of bed-parallel pressure solution seams is enhanced in rocks with high porosity; these authors, in fact, consider pores able to localize stress on non porous areas of the rock. Probably, in the rocks studied in this article, other factors (i.e. clay content, grain characteristics) play the key role for PSS development.

8. Conclusions

The results of a field and laboratory study conducted on Oligo-Miocene, ramp carbonates (skeletal grainstones and packstones, marly wackestones to mudstones) of the Bolognano Formation, show the control exerted by compositional, sedimentological and pore network characteristics on the development and distribution of burial-related, bed-parallel compaction bands and pressure solution seams. Specifically,

(i) bed-parallel compaction bands formed only within poorly cemented, porous grainstones (2D porosity $>$ 10%; 3D porosity $>$ 15%). Their dimensional parameters (i.e., length, spacing, thickness) were strongly controlled by both sorting and sphericity of the carbonate grains, as well as by the amount of intergranular macroporosity. All these rock characteristics enhanced all physical processes (i.e. grain rotation, translation and fracturing) associated to compaction banding;
(ii) bed-parallel pressure solution seams predominantly formed within fine-grained packstones made up of small amounts of clayish matrix (2–4% of total rock volume) and well-sorted and spherical carbonate grains with absence of internal pores. High contents of pre-existing cement enhanced intergranular pressure solution;
(iii) well-sorted carbonates with spherical grains may be suitable to both compaction banding and pressure solution;
(iv) skeletal grain types which compose grain-supported carbonate rocks (grainstones and packstones), in many cases, indirectly influence the distribution of both bed-parallel compaction bands and pressure solution seams.

Moreover, a link between the depositional paleoenvironments, and related depositional processes responsible for compositional, sedimentological and pore network characteristics of the studied carbonate rocks and the relative development and distribution of burial-related, bed-parallel structures, could be considered. Actually, carbonates deposited in high-energy environments (i.e. middle to proximal outer ramp; Fig. 6), consisting of well-sorted, coarser-grained rocks (i.e. grainstones) characterized by high values of well-connected, uniformly distributed, intergranular macroporosity, are more suitable to undergo to compaction banding. Whereas, carbonates deposited in transitional zones between high and low energy environments (i.e. intermediate outer ramp; Fig. 6), are more suitable to undergo to pressure solution, being made up of fine-grained rocks (i.e. grainstones to packstones) characterized by well-sorted spherical grains with small amounts of clay. These peculiar rock characteristics are due to the contemporaneous deposition of (i) carbonate skeletal sediments involved in a long transport determining efficient selection, breaking and rounding of grains, by action of distal bottom currents, and (ii) small amount of clayish mud by decantation (Fig. 6).

Considering that the containment and migration capacity of geofluids in the subsurface within carbonate rocks is strongly influenced by the distribution of compaction bands and pressure solution seams, the results of this research provide new tools useful to improve the prediction of reservoir quality by mapping/simulating/assessing carbonate facies.

Acknowledgments

We thank the Editor, Prof. Cees W. Passchier, Patrick Baud and one anonymous reviewer for their elaborate and constructive reviews of the manuscript. We also thank Mauro Alessandroni and Paolo Vallesi for their help during field work. This work has been supported by the Reservoir Characterization Project (www.rechproject.com) and by the MIUR, Prin 2009 (National Coordinator Emanuele Tondi).

References

Agosta, F., Kirschner, D.L., 2003. Fluid conduits in carbonate-hosted seismogenic normal faults of Central Italy. Journal of Geophysical Research 108 (B4), 2221. doi:10.1029/2002JB002013.

Agosta, F., Mulch, A., Chamberlain, P., Aydin, A., 2008. Geochemical traces of CO_2-rich fluid flow along normal faults in central Italy. Geophysical Journal International 174, 758–770. doi:10.1111/j.1365-246X.2008.03792.x.

Agosta, F., Alessandroni, M., Tondi, E., Aydin, A., 2009. Oblique normal faulting along the northern edge of the Majella anticline, central Italy: inferences on hydrocarbon migration and accumulation. Journal of Structural Geology 31, 674–690. doi:10.1016/j.jsg.2010.10.007.

Agosta, F., Alessandroni, M., Antonellini, M., Tondi, E., Giorgioni, M., 2010. From fractures to flow: a field-based quantitative analysis of an outcropping carbonate reservoir. Tectonophysics 490, 197–213. doi:10.1016/j.tecto.2010.05.005.

Aharonov, E., Katsman, R., 2009. Interaction between pressure solution and clays in stylolite development: insights from modeling. American Journal of Science 309, 607–632. doi:10.2475/07.2009.04.

Andrews, L.M., Railsback, L.B., 1997. Controls on stylolite development: morphologic, lithologic, and temporal evidence from bedding-parallel and transverse stylolites from the US appalachians. Journal of Geology 105, 59–73. doi:10.1086/606147.

Anselmetti, F.S., Luthi, S., Eberli, G.P., 1998. Quantitative characterization of carbonate pore systems by digital image analysis. AAPG Bulletin 81, 1815–1836.

Antonellini, M., Aydin, A., 1994. Effect of faulting on fluid flow in porous sandstones: petrophysical properties. AAPG Bulletin 78, 355–377. doi:10.1016/0148-9062(96)83981-7.

Antonellini, M., Tondi, E., Agosta, F., Aydin, A., Cello, G., 2008. Failure modes in deep-water carbonates and their impact for fault development: Majella Mountain, Central Apennines, Italy. Marine and Petroleum Geology 25, 1074–1096. doi:10.1016/j.marpetgeo.2007.10.008.

Aydin, A., 1978. Small faults formed as deformation bands in sandstone. Pureand Applied Geophysics 116, 913–930. doi:10.1007/BF00876546.

Aydin, A., 2000. Fractures, faults, and hydrocarbon entrapment, migration and flow. Marine and Petroleum Geology 17, 797–814. doi:10.1016/S0264-8172(00)00020-9.

Aydin, A., Ahmadov, R., 2009. Bed-parallel compaction bands in aeolian sandstone: their identification and characterization. Tectonophysics 479, 277–284. doi:10.1016/j.tecto.2009.08.033.

Aydin, A., Borja, R.I., Eichhubl, P., 2006. Geological and mathematical framework for failure modes in granular rock. Journal of structural Geology 28, 83–98. doi:10.1016/j.jsg.2005.07.008.

Aydin, A., Antonellini, M., Tondi, E., Agosta, F., 2010. Deformation along the leading edge of the Majella thrust sheet in central Italy. Journal of Structural Geology 32, 1291–1304. doi:10.1016/j.jsg.2008.10.005.

Bathurst, R.G.C., 1958. Diagenetic fabrics in some British Dinantian limestones. Liverpool and Manchester Geology 2, 1–36. doi:10.1002/gj.3350020103.

Bathurst, R.G.C., 1993. Microfabrics in Carbonate Diagenesis, a Critical Look at Forty Years in Research. In: Rezak, R., Iavoie, D.I. (Eds.), Carbonate Microfabrics. Springer-Verlag, New York, pp. 3–14.

Bathurst, R.G.C., 1995. Burial diagenesis of limestones under simple overburden. Stylolites, cementation, and feedback. Bulletin de la Societé Géologique de France 166, 181–192.

Baud, P., Schubnel, A., Wong, T.F., 2000. Dilatancy, compaction, and failure mode in Solnhofen limestone. Journal of Geophysical Research – Solid Earth 105 (B8), 19289–19303. doi:10.1029/2000JB900133.

Baud, P., Klein, E., Wong, T.F., 2004. Compaction localization in porous sandstones: spatial evolution of damage and acoustic emission activity. Journal of Structural Geology 26, 603–624. doi:10.1016/j.jsg.2003.09.002.

Baud, P., Vinciguerra, S., David, C., Cavallo, A., Walker, E., Reuschle, T., 2009. Compaction and failure in high porosity carbonates: mechanical data and microstructural observations. Pure Applied Geophysics 166, 869–898. doi:10.1007/s00024-009-0493-2.

Bjørlykke, K., Høeg, K., 1997. Effects of burial diagenesis on stresses, compaction and fluid flow in sedimentary basins. Marine and Petroleum Geology 14, 267–276. doi:10.1016/S0264-8172(96)00051-7.

Brown, A., 1997. Porosity variation in carbonates as a function of depth: Mississippian Madison Group, Williston Basin. In: Kupecz, J.A., Gluyas, J.G., Bloch, S. (Eds.), Reservoir Quality Prediction in Sandstone and Carbonates. AAPG Memoir, vol. 69, pp. 29–45.

Brzesowsky, R.H., Spiers, C.J., Peach, C.J., Hangx, S.J.T., 2011. Failure behavior of single sand grains: theory versus experiment. Journal of Geophysical Research 116, B06205. doi:10.1029/2010JB008120.

Cilona, A., Baud, P., Tondi E., Agosta F., Vinciguerra S., Rustichelli A., Spiers C.J. Deformation bands in porous carbonate grainstones: field and laboratory observations. Journal of Structural Geology, submitted for publication.

Davison, I., Alsop, I., Evans, N., Safaricz, M., 2000. Overburden deformation patterns and mechanisms of salt diapir penetration in the Central Graben, North Sea. Marine and Petroleum Geology 17, 601–618. doi:10.1016/S0264-8172(00)00011-8.

Ehrenberg, S.N., 2006. Porosity destruction in carbonate platforms. Journal of Petroleum Geology 29, 41–52. doi:10.1111/j.1747-5457.2006.00041.x.

Ehrenberg, S.N., Nadeau, P.H., 2005. Sandstone vs. Carbonate petroleum reservoirs: a global perspective on porosity-depth and porosity-permeability relationships. AAPG Bulletin 89, 435–445. doi:10.1306/11230404071.

Ehrenberg, S.N., Nadeau, P.H., Steen, O., 2009. Petroleum reservoir porosity versus depth: influence of geological age. AAPG Bulletin 93, 1281–1296. doi: 10.1306/06120908163.

Eichhubl, P., Hooker, J.N., Laubach, S.E., 2010. Pure and shear-enhanced compaction bands in Aztec Sandstone. Journal of Structural Geology 32, 1873–1886. doi:10.1016/j.jsg.2010.02.004.

Ferrill, D.A., Groshong Jr., R.H., 1993. Deformation conditions in the northern Subalpine Chain, France, estimated from deformation modes in coarse-grained limestone. Journal of Structural Geology 15, 995–1006. doi: 10.1016/0191-8141(93)90172-7.

Fletcher, R., Pollard, D., 1981. Anticrack model for pressure solution seams. Geology 9, 419–424. doi: 10.1130/0091-7613(1981)9<419:AMFPSS>2.0.CO;2.

Flügel, E., 2004. Microfacies of Carbonate Rocks. Analysis, Interpretation and Application. Springer-Verlag, Berlin, Heidelberg, New York.

Folk, L.R., Ward, W., 1957. Brazos river bar: a study in the significance of grain size parameters. Journal of Sedimentary Research 27, 3–26. doi:10.1306/74D70646-2B21-11D7-8648000102C1865D.

Fossen, H., Schultz, R., Shipton, Z., Mair, K., 2007. Deformation bands in sandstone - a review. Geological Society of London 164, 755–769. doi:10.1144/0016-76492006-036.

Gallagher, J.J., 1987. Fractography of sand grains broken by uniaxial compression. In: Marshall, J.R. (Ed.), Classic Particles. Van Nostrand Reinhold, New York, pp. 189–228.

Ghisetti, F., Vezzani, L., 1997. Geometrie deformative ed evoluzione cinematica dell'Appennino centrale. Studi Geologici Camerti 14, 127–154.

Ghisetti, F., Vezzani, L., 2002. Normal faulting, extension and uplift in the outer thrust belt of the central Apennines (Italy): role of the Caramanico fault. Basin Research 14, 225–236. doi:10.1046/j.1365-2117.2002.00171.x.

Graham, B., Antonellini, M., Aydin, A., 2003. Formation and growth of normal faults in carbonates within a compressive environment. Geology 31, 11–14. doi:10.1130/0091-7613(2003)031<0011:FAGONF>2.0.CO;2.

Gross, M.R., Fischer, M.P., Engelder, T., Greenfield, R.J., 1995. Factors controlling joint spacing in interbedded sedimentary rocks: interpreting numerical models with field observations from the Monterey Formation, USA. In: Ameen, M.S. (Ed.), Fractography: Fracture Topography as a Tool in Fracture Mechanics and Stress Analysis. Special Publication, vol. 92. Geological Society of America, pp. 215–233.

Halley, R.B., Schmoker, J.W., 1983. High porosity Cenozoic carbonate rocks of south Florida: progressive loss of porosity with depth. AAPG Bulletin 67, 191–200. doi:10.1017/S0016756800006555.

Heydari, E., 2000. Porosity loss, fluid flow, and mass transfer in limestone reservoirs: application to the upper Jurassic smackover formation, Mississippi. AAPG Bulletin 84, 100–118. doi:10.1306/040101851681.

Huang, Q., Angelier, J., 1989. Fracture spacing and its relation to bed thickness. Geological Magazine 126, 355–362. doi:10.1017/S0016756800006555.

Longiaru, S., 1987. Visual comparators for estimating the degree of sorting from plane and thin sections. Journal of Sedimentary Petrology 57, 791–794. doi:10.1306/212F8C60-2B24-11D7-8648000102C1865D.

Louis, L., Baud, P., Wong T-, F., 2007. Characterization of pore space heterogeneity and strain localization by X-ray computed tomography. Geological Society of London, Special Publication 284, 127–146. doi:10.1144/SP284.9.

Marchegiani, L., Van Dijk, J.P., Gillespie, P.A., Tondi, E., Cello, G., 2006. Scaling properties of the dimensional and spatial characteristics of fault and fracture systems in the Majella Mountain, central Italy. In: CelloG., MalamudB (Eds.), Fractal Analysis for Natural Hazards. Geological Society of London, Special Publication, vol. 261, pp. 113–131. doi:10.1144/GSL.SP.2006.261.01.09.

Merino, E., Ortoleva, P., Strickholm, P., 1983. Generation of evenly-spaced pressure-solution seams during (late) diagenesis: a kinetic theory. Contributions to Mineralogy and Petrology 82, 360–370. doi:10.1007/BF00399713.

Mollema, P.N., Antonellini, M.A., 1996. Compaction bands: a structural analog for anti-mode I cracks in Aeolian sandstone. Tectonophysics 267, 209–228. doi:10.1016/S0040-1951(96)00098-4.

Mutti, M., 1995. Porosity development and diagenesis in the Orfento supersequence and its bounding unconformities (Upper Cretaceous, Montagna della Majella, Italy). AAPG, Special Publication 63, 141–158.

Mutti, M., Bernoulli, D., Stille, P., 1997. Temperate carbonate platform drowning linked to Miocene oceanographic events: Maiella platform margin, Italy. Terra Nova 9, 122–125. doi:10.1046/j.1365-3121.1997.d01-19.

Ori, G.G., Roveri, M., Vannoni, F., 1986. Plio-Pleistocene sedimentation in the Apennine–Adriatic foredeep (central Adriatic Sea, Italy). In: Allen, P.A., Homewood, P. (Eds.), Foreland Basins. Blackwell, Oxford, pp. 183–198. doi:10.1002/9781444303810.ch9.

Ortega, O.J., Marrett, R.A., Laubach, S.E., 2006. A scale-independent approach to fracture intensity and average spacing measurement. AAPG Bulletin 90, 193–208. doi:10.1306/08250505059.

Park, W.C., Schot, E.K., 1968. Stylolites: their nature and origin. Journal of Sedimentary Petrology 38, 175–191. doi:10.1306/74D71910-2B21-11D7-8648000102C1865D.

Passchier, C.W., Trouw, R.A.J., 1996. Microtectonics. Springer-Verlag, Berlin.

Paterson, M.S., 1995. A theory for granular flow accommodated by material transfer via an intergranular fluid. Tectonophysics 245, 135–152. doi:10.1016/0040-1951(94)00231-W.

Petit, J.P., Mattauer, M., 1995. Palaeostress superimposition deduced from mesoscale structures in limestone: the Matelles exposure, Languedoc, France. Journal of Structural Geology 17, 245–256. doi:10.1016/0191-8141(94)E0039-2.

Pomar, L., Brandano, M., Westphal, H., 2004. Miocene tropical foramol-rhodalgal-bryomol associations of the western Mediterranean – a critical review. Sedimentology 51, 627–651. doi:10.1111/j.1365-3091.2004.00640.x.

Rath, A., Exner, U., Tschegg, C., Grasemann, B., Laner, R., Draganits, E., 2011. Diagenetic control of deformation mechanisms in deformation bands in a carbonate grainstone. AAPG Bulletin 95, 1369–1381. doi:10.1306/01031110118.

Renard, F., Ortoleva, P., Gratier, J.P., 1997. Pressure solution in sandstones: influence of clays and dependence on temperature and stress. Tectonophysics 30, 257–266. doi:10.1016/S0040-1951(97)00039-5.

Renard, F., Dysthe, D., Feder, J., Bjørlykke, K., Jamtveit, B., 2001. Enhanced pressure solution creep rates induced by clay particles: experimental evidence in salt aggregates. Geophysical Research Letters 28, 1295–1298. doi:10.1029/2000GL012394.

Renard, F., Schmittbuhl, J., Gratier, J.P., Meakin, P., Merino, E., 2004. The three-dimensional morphology of stylolites: roughness analysis and possible genetic implications. Journal of Geophysical Research 109, B03209. doi:10.1029/2003JB002555.

Rustichelli, A., 2010. Mechanical stratigraphy of carbonate rocks: examples from the Maiella Mountain (central Italy) and the Granada Basin (southern Spain). Ph.D thesis, University of Camerino.

Rutter, E.H., 1976. The kinetics of rock deformation by pressure solution. Philosophical Transactions of the Royal Society of London 283, 203–219. doi:10.1098/rsta.1976.0079.

Schmoker, J.W., Halley, R.B., 1982. Carbonate porosity vs. depth: a predictable relation for south Florida. AAPG Bulletin 66, 2561–2570.

Schultz, R.A., 2009. Scaling and paleodepth of compaction bands, Nevada and Utah. Journal of Geophysical Research 114, B03407. doi:10.1029/2008JB005876 33.

Scisciani, V., Tavarnelli, E., Calamita, F., 2002. The interaction of extensional and contractional deformation in the outer zones of the Central Apennines, Italy. Journal of Structural Geology 24, 1647–1658. doi:10.1016/S0191-8141(01)00164-X.

Sibley, D.F., Blatt, H., 1976. Intergranular pressure solution and cementation of the Tuscarora Orthoquartzite. Journal of Sedimentary Petrology 46, 881–896. doi:10.1306/212F7081-2B24-11D7-8648000102C1865D.

Tada, R., Siever, R., 1989. Pressure solution during diagenesis. Annual Reviews of Earth and Planetary Science 17, 89–118. doi:10.1146/annurev.ea.17.050189.000513.

Tembe, S., Baud, P., Wong, T.F., 2008. Stress conditions for the propagation of discrete compaction bands in porous sandstone. Journal of Geophysical Research 113, B09409. doi:10.1029/2007JB005439.

Tondi, E., 2007. Nucleation, development and petrophysical properties of faults in carbonate grainstones: evidence from the San Vito Lo Capo peninsula (Sicily, Italy). Journal of Structural Geology 29, 614–628. doi:10.1016/j.jsg.2006.11.006.

Tondi, E., Antonellini, M., Aydin, A., Marchegiani, L., Cello, G., 2006. The role of deformation bands and pressure solution seams in fault development in carbonate grainstones of the Majella Mountain, Italy. Journal of Structural Geology 28, 376–391. doi:10.1016/j.jsg.2005.12.001.

Tondi, E., Cilona, A., Agosta, F., Aydin, A., Rustichelli, A., Renda, P., Giunta, G. Growth processes, dimensional parameters and scaling relationships of two conjugate sets of compactive shear bands in porous carbonate grainstones, Favignana Island, Italy. Journal of Structural Geology, in press.

Vajdova, V., Baud, P., Wong, T.F., 2004. Compaction, dilatancy, and failure in porous carbonate rocks. Journal of Geophysical Research-Solid Earth 109, B5. Article no. B05204doi:10.1029/2003JB002508.

Vajdova, V., Zhu, W., Chen, T.M.N., Wong, T.F., 2010. Micromechanics of brittle faulting and cataclastic flow in Tavel limestone. Journal of Structural Geology 32, 1158–1169. doi:10.1016/j.jsg.2010.07.007.

Vajdova, V., Baud P., Wu L., Wong T.F. Micromechanics of inelastic compaction in two allochemical limestones. Journal of Structural Geology, 33, in press.

Vecsei, A., 1991. Aggradation un Progradation eines karbonatplatform-Randes: Kreide bis Mittleres Tertiär der Montagna della Maiella, Abruzzen. In: Mitteilungen aus dem Geologischen Institut der Eidgenössischen Technischen Hochschule und der Universitat Zürich. Neue Folge 294.

Vecsei, A., Sanders, D., 1999. Facies analysis and sequence stratigraphy of a Miocene warm-temperate carbonate ramp, Montagna della Maiella, Italy. Sedimentary Geology 23, 103–127. doi:10.1016/S0037-0738(98)00079-7.

Vezzani, L., Ghisetti, F., 1998. Carta Geologica Dell'Abruzzo. S.EL.CA, Firenze.

Westphal, H., Halfar, J., Freiwald, A., 2010. Heterozoan carbonates in subtropical to tropical settings in the present and past. International Journal of Earth Sciences 99, 1–17. doi:10.1007/s00531-010-0563-9.

Weyl, P.K., 1959. Pressure solution and the force of crystallization. A phenomenological theory. Journal of Geophysical Research 64, 2001–2025. doi:10.1029/JZ064i011p02001.

Zhang, X., Spiers, C.J., 2005. Compaction of granular calcite by pressure solution at room temperature and effects of pore fluid chemistry. International Journal of Rock Mechanics and Mining Sciences 42, 950–960. doi:10.1016/j.ijrmms.2005.05.017.

Zhang, J., Wong, T.F., Davis, D.M., 1990. Micromechanics of pressure induced grain crushing in porous rocks. Journal of Geophysical Research 95, 341–352. doi:10.1029/JZ064i011p02001.

Zhu, W., Baud, P., Wong, T.F., 2010. Micromechanics of cataclastic pore collapse in limestone. Journal of Geophysical Research 115, B04405. doi:10.1029/2009JB006610.